

Chapter 4. Results and Discussion

In this Chapter, results from various geochemical and isotopic investigations are presented both in tabular and graphical forms and salient features of the observed variations are described. This is followed by the interpretation and discussion leading to specific conclusions.

4.1 Results

4.1.1 Groundwater Helium and Temperature

Details of (i) the sampled well locations; (ii) well type; values of (iii) 'Excess helium' concentration (He_{ex}); and (iv) temperature of groundwater are given in Table 4.1. A map showing isolines of He_{ex} in groundwater (see Section 2.6.2 for definition of excess helium) of the NGC region is given in Figure 4.1. The isolines of groundwater temperature are shown in Figure 4.2.

Of the 12 soil-gas samples analyzed, only one sample ~100 m away from the thermal springs of Tuwa showed helium concentration (7.0 ppmv) higher than the atmospheric background. All other soil gas samples had helium concentrations close to atmospheric value.

It is seen from Figure 4.1 that groundwater with very high values of He_{ex} is found in the region west of the WCBBF where a set of intersecting orthogonal basement faults are located (See Figure 1.3). The highest He_{ex} value (2843 ppmAEU) was observed at Zinzawadar (CBGW-120; Table 4.1; Figure 4.1) located close to the western extremity of the longest orthogonal fault cutting across Cambay Basin. High He_{ex} in groundwater is also found at some locations on the eastern flank of the Cambay basin, associated with thermal springs of Lasundra (L) and Tuwa (T). The highest He_{ex} value (1163 ppmAEU) on the east flank of Cambay basin was observed in a groundwater sample from a hand pump near the thermal spring at Tuwa, located close to the Aravalli foothills (CBGW-21; Table 4.1; Figure 4.1). It is also seen from Figure 4.1 that the isoline of 5 ppmAEU He_{ex} lies close to the WCBBF.

The groundwater temperature in the study area ranged from 28°–61°C with an average value of 30°C. It is seen from Figure 4.2 that within the Cambay basin (having thick sedimentary cover), the groundwater temperatures are around 30°C. Along the WCBBF and on the west flank of Cambay basin a large area shows high groundwater temperature (>35°C), associated with thermal artesian wells and thermal springs. On the east flank, the groundwater temperatures >40°C are seen in and around the thermal springs tapping the Precambrian granitic basement. The highest groundwater

temperature (61°C) was found in one of the eight sampled vents (CBGW-18; Table 4.1) of the thermal springs at Tuwa (T).

Table 4.1 Details of groundwater sampling sites together with values of He_{ex} and calculated ⁴He ages using helium release factor (Λ_{He}) of 1 and 0.4. Calculations of ⁴He ages are based on Th = 7.54±3.5; U = 1.07±0.41; ρ = 2.6 g cm⁻³; n = 20%. [TW = tubewell; DCB = dug cum bore; DW = dug well; HP = handpump; TA = thermal artesian; TS = thermal spring; He_{ex} = (measured – 5.3) ppmAEU].

CBGW Sample no.	Location name	Well type	Lat. (°N)	Long. (°E)	Depth bgl (m)	Temp. (°C)	He _{ex} ppmAEU	⁴ He ages (kaBP) (Λ _{He} = 1)	⁴ He ages (kaBP) (Λ _{He} = 0.4)
1	Gandhinagar	TW	23.24	72.68	55	---	0	0	0
2	Prantij	DCB	23.44	72.85	18	---	0	0	0
3	Prantij	TW	23.45	72.86	30	---	0	0	0
4	Shikha	DCB	23.39	73.23	30	---	0	0	0
5	Bayad	TW	23.22	73.21	18	---	0	0	0
6	Gundela	DW	23.12	73.36	9	---	0	0	0
7	Rojawa	TW	22.91	73.33	34	---	0	0	0
8	Lasundra	DW	22.91	73.14	6	52	186	547	1368
9	Lasundra	DW	22.91	73.14	6	---	55	162	404
10	Sinhuji	DCB	22.82	72.86	24	---	0	0	0
11	Dakore	TW	22.76	73.16	37	---	0	0	0
12	Ladvel	HP	22.91	73.12	12	---	0.2	1	1
13	Kapadvanj	DCB	23.04	73.10	38	---	0	0	0
14	Kunha	TW	23.01	72.77	91	---	0	0	0
15	Lasundra	TW	22.92	73.15	85	---	221	650	1625
16	Anghadi	DCB	22.81	73.30	24	---	0	0	0
17	Timba	HP	22.82	73.40	12	---	0	0	0
18	Tuwa	TS	22.80	73.46	1	61	137	403	1007
19	Tuwa	TS	22.80	73.46	1	47	96	282	706
20	Tuwa	TS	22.80	73.46	1	28	475	1397	3493
21	Tuwa	HP	22.80	73.46	12	51	1163	3421	8551
22	Tuwa	DW	22.80	73.46	6	---	0	0	0
23	Godhara	DW	22.78	73.60	7	---	0	0	0
24	Godhara	TW	22.76	73.61	30	---	0	0	0
25	Baska	HP	22.47	73.45	18	---	0	0	0
26	Baroda	TW	22.27	73.19	30	---	0	0	0
27	Jarod	HP	22.44	73.35	12	---	0	0	0
28	Khadki	HP	22.65	73.52	12	---	0	0	0
29	Dabhoi	HP	22.13	73.41	12	---	0	0	0
30	Sathod	TW	22.07	73.38	53	---	0	0	0
32	Adalaj	TW	23.17	72.58	229	---	0.1	0	1
33	Kalol	TW	23.26	72.47	183	---	0.1	0	1
34	Malharpur	HP	22.81	72.62	18	---	0.1	0	1
35	Marala	DCB	22.62	72.64	30	---	0.1	0	1
36	Khambhat	TW	22.33	72.62	91	---	0.8	2	6
37	Nadiad	TW	22.56	72.82	30	---	0.1	0	1
38	Bhadran	TW	22.37	72.9	67	---	0.4	1	3
39	Masar Rd.	TW	22.11	72.89	61	---	5.2	15	38

Table 4.1 continues

CBGW Sample no.	Location name	Well type	Lat. (°N)	Long. (°E)	Depth bgl (m)	Temp. (°C)	He _{ex} ppmAEU	⁴ He ages (kaBP) ($\Delta_{He}=1$)	⁴ He ages (kaBP) ($\Delta_{He}=0.4$)
40	Kalak	DCB	22.02	72.76	21	---	0.1	0	1
43	Manglej	TW	22.09	73.17	76	---	0.1	0	1
44	Dholka	TW	22.69	72.43	107	---	0.5	1	4
45	Dholera	TA	22.25	72.19	168	43	109	321	801
50	Rampara	TW	22.11	71.89	76	---	2.7	8	20
51	Dhandhuka	DCB	22.38	71.98	15	---	0.2	1	1
52	Bawala	TW	22.83	72.36	198	33	6.3	19	46
53	Bagodra	TA	22.64	72.2	335	41	88	259	647
54	Bagodra	TA	22.64	72.2	335	41	190	559	1397
55	Gundi	TA	22.55	72.23	290	40	234	688	1721
56	Batod	HP	22.16	71.66	37	---	0.1	0	1
58	Vejalka	DCB	22.4	71.72	53	---	6.3	19	46
59	Wadhwan	TW	22.72	71.68	91	35	0.2	1	1
60	Bajana	TW	23.12	71.78	175	---	16	47	118
61	Dashada	TW	23.32	71.84	168	---	49	144	360
62	Sachana	TW	23.08	72.17	21	34	2.7	8	20
63	Vithalpur	TW	23.37	72.05	198	---	1	3	7
64	Umerkhaya	DW	22.90	72.02	13	---	0.2	1	1
65	Shiyala	TA	22.70	72.16	274	38	73	215	537
66	Ruhika	TA	22.66	72.23	457	41	157	462	1154
67	Sarala	TA	22.67	72.2	274	40	89	262	654
68	Vithalgadh	DW	22.99	71.97	15	---	0.2	1	1
69	Nardipur	TW	23.25	72.56	200	29	0	0	0
70	Santej	TW	23.11	72.47	274	29	0	0	0
71	Rancharda	TW	23.08	72.45	213	---	0	0	0
72	Nardipur	TW	23.25	72.56	200	29	0	0	0
73	Santej	TW	23.11	72.47	274	29	0	0	0
74	Rancharda	TW	23.08	72.45	213	---	0	0	0
75	Ananddham	TW	22.99	72.52	--	---	0	0	0
76	Sarkhej	TW	22.99	72.49	91	---	0	0	0
77	Sarkhej	TW	22.99	72.49	18	---	0	0	0
78	Collet	TW	22.97	72.43	229	33	1	3	7
79	Collet	TW	22.98	72.44	61	30	0	0	0
80	Sanand	TW	23.00	72.38	229	29	0.4	1	3
81	Thol	TW	23.13	72.38	183	32	0	0	0
82	Thol	HP	23.15	72.37	24	31	0	0	0
83	Rangpurda	TW	23.25	72.30	183	31	0.5	1	4
84	Kadi	TW	23.30	72.31	213	31	0	0	0
85	Bhoyani	TW	23.36	72.23	244	32	0.4	1	3
86	Katosan Road	TW	23.40	72.24	244	32	0.4	1	3
87	Navdeep Ind.	TW	23.01	72.34	244	30	0.8	2	6
88	Vansa	DCB	23.02	72.33	244	28	0.1	0	1
89	Sachana	TW	23.08	72.16	12	39	34	100	250
90	Hansalpur	TW	23.10	72.07	213	33	22	65	162
91	Viramgam	TW	23.10	72.06	110	34	66	194	485
92	Juna Padhar	TW	23.19	72.04	229	40	62	182	456
93	Endla	TW	23.29	72.04	244	38	23	68	169
94	Sitapur	TW	23.45	71.99	265	34	16	47	118

Table 4.1 continues

CBGW Sample no.	Location name	Well type	Lat. (°N)	Long. (°E)	Depth bgl (m)	Temp. (°C)	He _{ex} ppmAEU	⁴ He ages (kaBP) ($\Delta_{He}=1$)	⁴ He ages (kaBP) ($\Delta_{He}=0.4$)
95	Sitapur	TW	23.44	71.98	183	38	21	62	154
96	Valevda	TW	23.46	71.94	299	32	2.8	8	21
97	Valevda	TW	23.45	71.94	213	40	17	50	125
98	Dhanap	TW	23.26	72.75	262	31	0.2	1	1
99	Majara	TW	23.36	72.8	213	29	0.1	0	1
100	Talod	TW	23.35	72.93	122	28	0	0	0
101	Tajpur Camp	HP	23.37	73.03	46	29	0.2	1	1
102	Vadagam	HP	23.33	73.17	24	29	0.2	1	1
103	Ramnagar	HP	23.39	73.23	9	28	0	0	0
104	Dhamanya	HP	23.34	73.25	14	29	0	0	0
105	Kamaliya	HP	23.33	73.31	30	28	0	0	0
106	Ranmalgadh	TW	22.98	72.34	61	33	0.7	2	5
107	Rethal	TW	22.88	72.19	152	34	12	35	87
108	Shahpur	HP	22.88	72.02	168	29	2	6	15
109	Vasvelia	TW	23.00	72.04	18	37	131	385	963
110	Bhojva	TW	23.15	72.03	168	31	2.3	7	17
111	Malanpur	TW	23.25	71.93	61	35	56	165	412
112	Zainabad	TW	23.26	71.68	274	34	112	329	824
113	Zainabad	HP	23.26	71.68	213	29	0	0	0
114	Zinzuvada	TW	23.35	71.65	15	35	31	91	228
115	Zinzuvada	HP	23.35	71.66	198	28	0	0	0
116	Changodar	HP	22.93	72.44	15	29	0.3	1	2
117	Kalayangdh	TW	22.72	72.27	9	27	1.4	4	10
118	Limbdi	HP	22.57	71.81	61	28	0	0	0
119	Vadod	TW	22.56	71.63	14	29	1.6	5	12
120	Zinzawadar	TW	22.45	71.69	53	34	2843	8362	20904
121	Zinzawadar	HP	22.45	71.69	285	29	0	0	0
122	Chuda	TW	22.49	71.69	46	31	1290	3794	9485
123	Vekaria	HP	22.82	72.06	183	29	0.4	1	3
124	Fulgam	HP	22.54	71.54	12	31	0.2	1	1
125	Shekhpur	TW	22.70	71.56	55	31	0.2	1	1
126	Vana	HP	22.87	71.71	55	---	0	0	0
127	Rangpur	DW	22.41	71.93	12	27	0.6	2	4
128	Vagad	DW	22.36	71.87	11	29	0	0	0
129	Nagnesh	TW	22.36	71.76	18	31	2	6	15
130	Nagnesh	HP	22.36	71.76	61	31	1.1	3	8
131	Alampur	DW	22.30	71.66	17	28	0	0	0
132	Paliyad	HP	22.25	71.56	46	30	0	0	0
133	Paliyad	TW	22.25	71.56	91	32	0.7	2	5
134	Botad	HP	22.17	71.66	49	---	0	0	0
135	Tatam	TW	22.06	71.62	64	31	0.8	2	6
137	Ahmedabad	TW	22.98	72.62	233	35	0	0	0
138	Hathijan	TW	22.94	72.64	137	35	0.5	1	4
139	Onthwari	DCB	22.82	72.80	61	35	0	0	0
140	Ran Na Muvada	DCB	22.84	72.95	85	35	3.6	11	26
141	Porda	DCB	22.92	73.00	67	33	0.2	1	1
147	Sarangpur	HP	22.16	71.77	61	34	0	0	0
149	Panavi	TW	22.08	71.89	125	41	1624	4776	11941
150	Keriya Dhal	TW	22.11	71.89	183	35	0	0	0
151	Vaya	DW	22.20	71.87	30	30	0	0	0

Table 4.1 continues

CBGW Sample no.	Location name	Well type	Lat. (°N)	Long. (°E)	Depth bgl (m)	Temp. (°C)	He _{ex} ppmAEU	⁴ He ages (kaBP) ($\Delta_{He}=1$)	⁴ He ages (kaBP) ($\Delta_{He}=0.4$)
152	Devthal	DCB	22.75	72.13	10	35	4.4	13	32
153	Devthal	TW	22.76	72.12	274	35	116	341	853
154	Kanera	TW	22.81	72.62	137	33	1.4	4	10
155	Sokhada	TW	22.74	72.68	98	34	0.3	1	2
156	Matar	TW	22.71	72.68	110	35	0.1	0	1
157	Nar	TW	22.48	72.71	107	35	0.7	2	5
158	Jogan	DCB	22.45	72.79	34	32	0.1	0	1
159	Bharel	TW	22.41	72.83	61	34	0.1	0	1
160	Dededa	DW	22.46	72.91	58	32	0.3	1	2
161	Anand	TW	22.53	72.96	46	32	0	0	0
162	Uttarsanda	TW	22.66	72.9	55	32	0	0	0
163	Sojitra	TW	22.55	72.74	140	35	1.8	5	13
164	Jedwapura	TW	22.55	72.83	91	34	0	0	0
165	Bedva	DCB	22.55	73.04	37	---	0	0	0
166	Ode	TW	22.62	73.11	47	32	0.7	2	5
167	Lingda	HP	22.69	73.08	20	31	0.5	1	4
168	Alindra	HP	22.70	72.97	55	34	0.5	1	4
169	Vaghasi	TW	22.54	73.00	49	---	0	0	0
170	Bhetasi	TW	22.43	73.02	61	33	0	0	0
171	Samiala	TW	22.26	73.12	113	33	0.1	0	1
172	Dabhasa	TW	22.25	73.05	76	34	0	0	0
173	Vadu	DCB	22.21	72.98	51	33	0.2	1	1
174	Vadu	TW	22.22	72.98	130	37	3.5	10	26
175	Gavasad	TW	22.19	72.97	130	35	0.1	0	1
176	Jambusar	TW	22.05	72.81	73	34	1	3	7
179	Karjan	TW	22.05	73.12	107	34	0	0	0
184	Kanara	TW	22.08	73.4	183	34	0	0	0
185	Mandwa	TW	22.01	73.43	46	35	0.1	0	1
186	Chandod	TW	22.99	73.46	122	34	0	0	0
187	Ankhi	TW	22.13	73.2	91	33	4.6	14	34
188	Kayavarohan	TW	22.08	73.24	99	33	0	0	0
189	Dantiwada	HP	24.17	72.48	36	34	0	0	0
190	Dantiwada	T	24.16	72.48	101	31.5	0.4	1	3
191	Gola	DCB	24.19	72.78	37	28	0.2	1	1
192	Dharoi	HP	24.00	72.85	12	29	0.1	0	0
193	Mumanvas	DW	24.04	72.83	18	27	0.4	1	3
194	Mathasur	HP	23.80	73.01	46	30	0.2	1	1
195	Himmat-nagar	HP	23.72	72.96	27	29	0.3	1	3
196	Dalpur	DCB	23.51	72.95	21	29	0	0	0
202	Math	HP	23.43	73.62	15	28	0.2	1	1
203	Aritha	HP	23.14	73.65	15	29	0.1	0	1
204	Limbodra	HP	23.19	73.60	15	29	0.3	1	2
205	Ghaliya Danti	HP	23.36	73.51	18	29	0.1	0	1
206	Shehra	HP	22.95	73.63	18	29	0.1	0	1
207	Popatpura	HP	22.79	73.45	18	29.5	0.2	1	1
208	Maniyor	TW	23.82	72.96	74	35	0.1	0	1
209	Dharewada	TW	23.98	72.39	212	35	2	6	15
210	Ganguva	TW	24.16	72.73	85	33	0	0	0
211	Chadotar	TW	24.21	72.39	63	32	0	0	0

Table 4.1 continues

CBGW Sample no.	Location name	Well type	Lat. (°N)	Long. (°E)	Depth bgl (m)	Temp. (°C)	He _{ex} ppmAEU	⁴ He ages (kaBP) ($\Delta_{He}=1$)	⁴ He ages (kaBP) ($\Delta_{He}=0.4$)
212	Bhadath	TW	24.34	72.2	141	32	0.3	1	2
213	Kuwarva	TW	24.04	71.9	187	35	0.3	1	2
214	Kuwarva	TW	24.05	71.9	122	33	0.3	1	2
215	Tharad	TW	24.41	71.64	299	42	30	88	221
216	Jitoda	TW	23.74	72.15	313	35	0.6	2	4
217	Jitoda	TW	23.74	72.15	427	42	9.7	29	71
218	Sami	TW	23.70	71.78	299	44	64	188	471
219	Wavadi	TW	23.92	72.52	145	34	0	0	0
220	Pilwai	TW	23.53	72.69	235	39	17	50	125
221	Pilwai	TW	23.54	72.68	152	37	0.5	1	4
222	Heduva	TW	23.57	72.34	267	37	1.8	5	13
223	Vaghpur	TW	23.68	73.42	86	33	23	68	169
224	Edla	TW	23.54	72.06	289	40	11	32	81
225	Sherisa	TW	23.20	72.48	232	35	0.3	1	2
312	Diyodar	TW	24.10	71.75	207	33	1.9	6	14
313	Diyodar	TW	24.10	71.75	207	33	1.2	4	9
314	Tharad	TW	24.41	71.64	201	39	30	88	221
316	Agathala	TW	24.29	71.88	137	31	0	0	0
317	Sujanipur	TW	23.89	72.11	91	31	0	0	0
318	Sujanipur	TW	23.90	72.12	326	37	16	47	118
319	Sujanipur	TW	23.91	72.12	40	29	0	0	0
320	Kuwarva	TW	24.04	71.9	187	32	0	0	0
321	Kharia	TW	23.94	71.83	158	30	0	0	0
322	Sami	TW	23.7	71.78	299	41	45	132	331
323	Hedva	TW	23.57	72.34	82	33	1.5	4	11
324	Kuder	TW	23.70	71.87	262	34	1.5	4	11
325	Patan	TW	23.84	72.11	198	31	0	0	0
326	Patan	TW	23.84	72.11	130	32	0	0	0
327	Patan	TW	23.84	72.11	60	29	0	0	0
328	Jitoda	TW	23.74	72.15	313	33	0.3	1	2
329	Jitoda	TW	23.74	72.15	448	39	10	29	74
330	Kamboi	TW	23.67	72.02	213	32	6.4	19	47
331	Muthia	TW	23.09	72.69	142	31	0.3	1	2
332	Paliya	TW	23.18	72.83	119	31	0.3	1	2
333	Punsari	TW	23.39	73.10	32	30	0	0	0
334	Dalani Muwadi	TW	23.36	72.88	91	31	12	35	88
335	Rojad	HP	23.35	73.09	29	29	0	0	0
336	Vadrad	TW	23.42	72.89	58	31	0	0	0
337	Tejpur	TW	23.39	72.81	160	30	0	0	0
338	Navapur	TW	23.60	72.90	122	32	0.6	2	4
339	Dhanap	TW	23.26	72.75	168	32	0	0	0
340	Indroda Park	TW	23.19	72.65	107	31	0.3	1	2
341	Rupawati	TW	23.00	72.30	213	37	0	0	0
342	Sokali	TW	23.10	72.11	93	32	0.6	2	4
343	Dudapur	TW	23.02	71.58	61	32	44	129	324
355	Salajada	TW	22.80	72.39		35	0.9	3	7
356	Salajada	TW	22.79	72.39	198	35	0.9	3	7
357	Salajada	TW	22.79	72.39	93	31	0	0	0
358	Gundi	TA	22.55	72.23	>290	42	178	524	1309
359	Shiyal	TA	22.68	72.16	274	42	230	676	1691

Table 4.1 continues

CBGW Sample no.	Location name	Well type	Lat. (°N)	Long. (°E)	Depth bgl (m)	Temp. (°C)	He _{ex} ppmAEU	⁴ He ages (kaBP) ($\Delta_{He}=1$)	⁴ He ages (kaBP) ($\Delta_{He}=0.4$)
360	Padgol	TW	22.59	72.84	137	32	1.4	4	10
361	Morad	TW	22.54	72.86	91	31	0	0	0
362	Gumadia	TW	22.76	73.23	49	31	0.3	1	2
363	Tuwa	TS	22.80	73.46	1	50	405	1191	2978
364	Tuwa	TS	22.80	73.46	1	43	229	674	1684
365	Tuwa	TS	22.80	73.46	1	36	265	779	1949
366	Tuwa	TS	22.80	73.46	1	33	253	744	1860
367	Dholera	TA	22.25	72.19	168	45	443	1303	3257

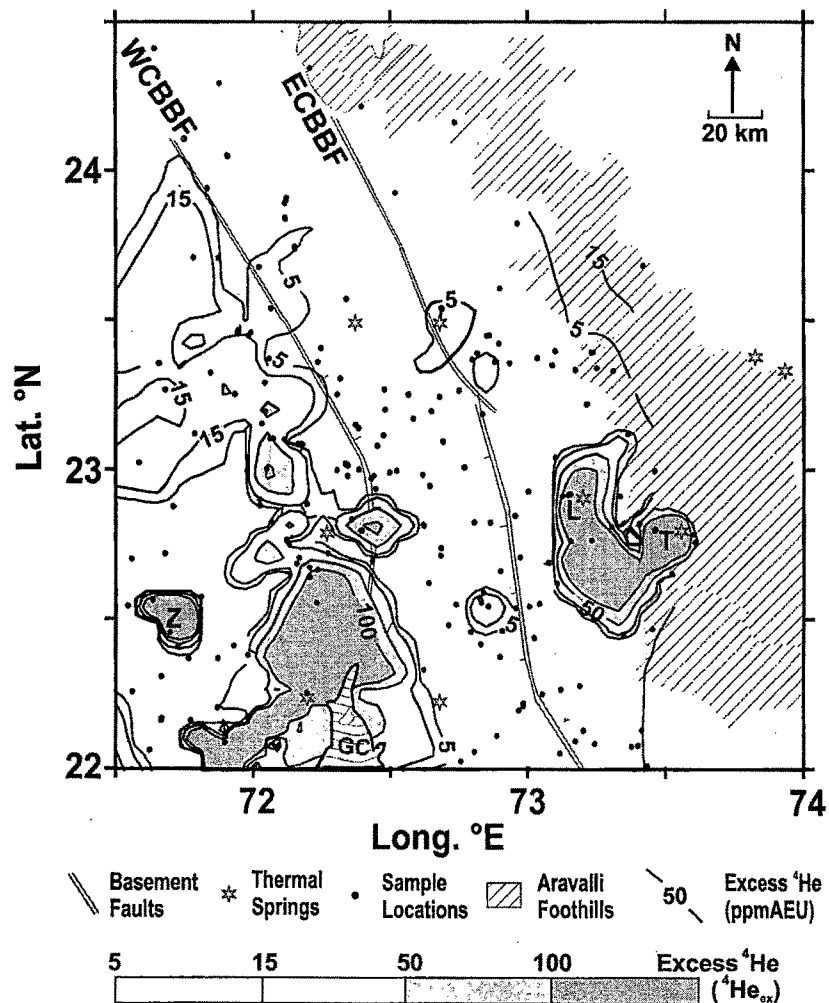


Figure 4.1 Isoline map of He_{ex} in groundwater of the NGC region. The isoline of 5 ppmAEU He_{ex} runs almost along the WCBBF. Pockets of He_{ex} >50 ppmAEU overlap with pockets of high (>40°C) groundwater temperature (Figure 4.2). Sampling locations are indicated by dots. L, T and Z respectively indicate the locations of thermal springs at Lasundra, Tuwa and a tubewell in Zinzawadar.

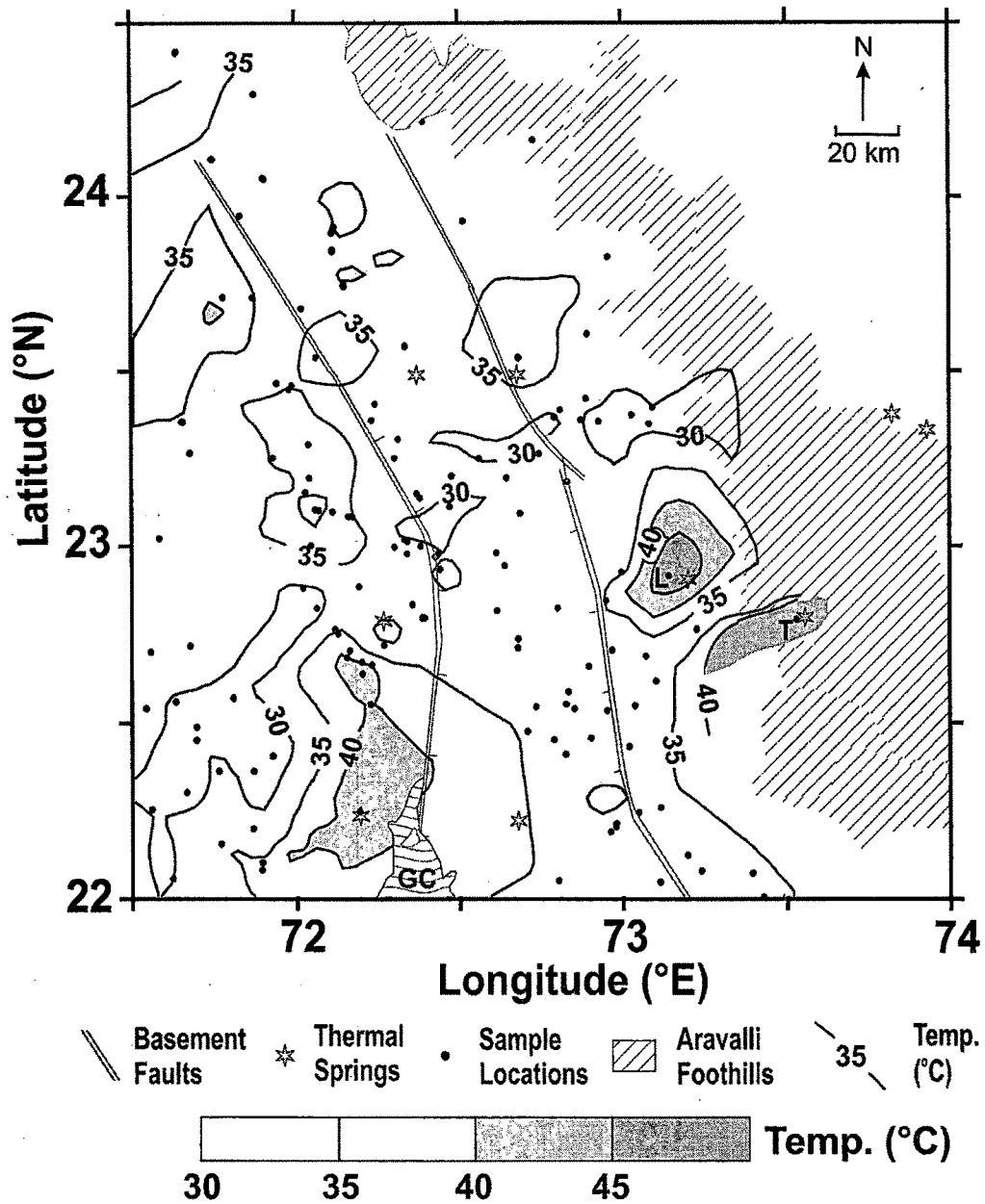


Figure 4.2 Isoline map of groundwater temperature in the NGC region. Large areas on both east and west flanks of the Cambay basin show groundwater temperature $>35^{\circ}\text{C}$. Temperatures $>40^{\circ}\text{C}$ are seen around thermal springs. Sampling locations are indicated by dots. L and T respectively indicate locations of thermal springs at Lasundra and Tuwa

It is seen from Figure 4.1 and Figure 4.2 that areas with very high He_{ex} (>50 ppm AEU) in groundwater overlap with areas having high ($>40^{\circ}\text{C}$) groundwater temperatures. In general, areas of high He_{ex} (>15 ppmAEU) are associated with high groundwater temperature ($>35^{\circ}\text{C}$). However, on a plot of He_{ex} vs. temperature (Figure 4.3) no

quantitative relationship is observed. It may also be noticed that even for different vents within the small region around the thermal springs at Tuwa no quantitative relationship is observed between temperatures (28°–61°C) and He_{ex} (137-475 ppmAEU). Also, no correlation was found between depth below ground level of sampled well and He_{ex} in groundwater in the NGC region (Figure 4.4).

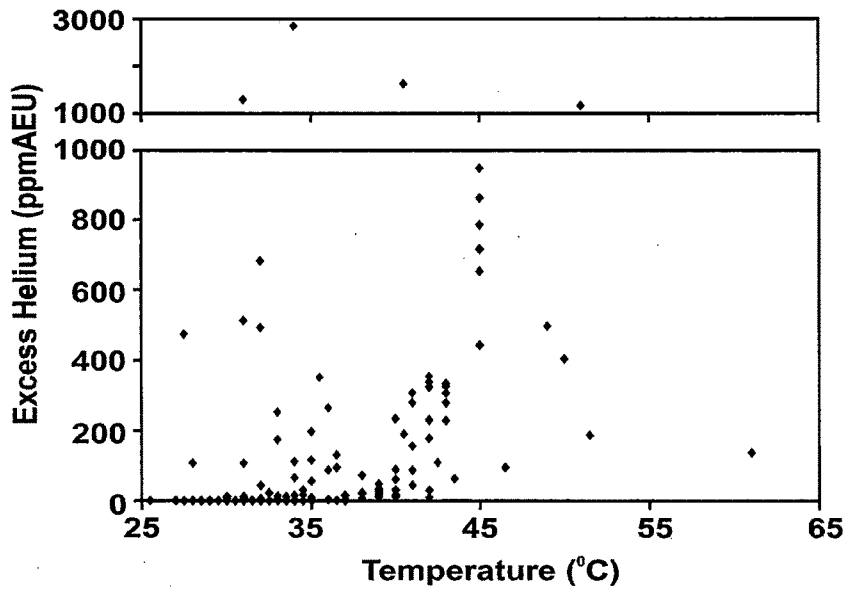


Figure 4.3 Groundwater temperature vs. He_{ex} in groundwater from NGC region.

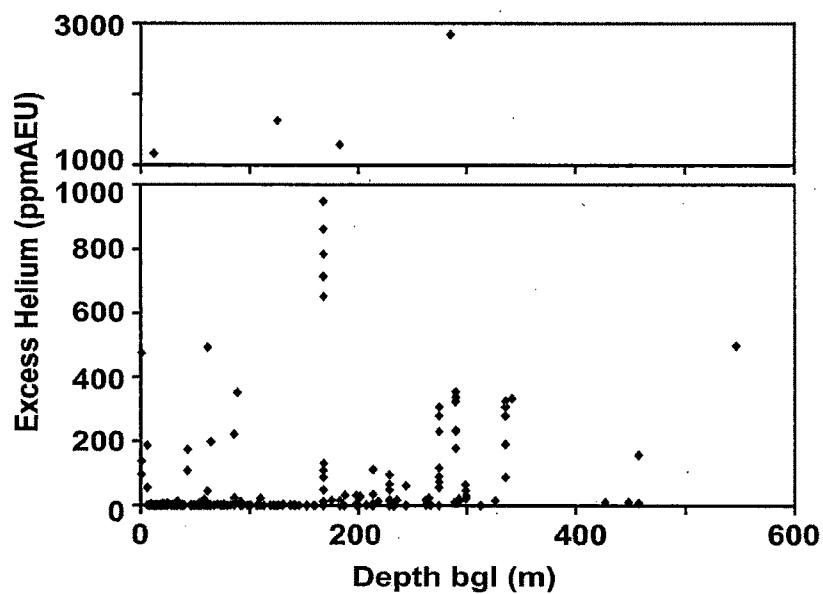


Figure 4.4 Depth of the sampled wells (bgl) vs. He_{ex} in groundwater in NGC region.

4.1.2 Groundwater Fluoride

Details of (i) the sampled well location; (ii) well type; and (iv) measured values of fluoride concentration are given in Table 4.2. The geographical distribution of fluoride in groundwater from the NGC region is shown in Figure 4.5.

Table 4.2 Details of groundwater sampling sites together with measured values of fluoride concentration and Electrical Conductivity. (TW = tubewell; DCB = dug cum bore; DW = dug well; HP = hand pump; TA = thermal artesian; TS = thermal spring; bgl = below ground level; CBGW = Cambay Basin Ground Water; EC = Electrical Conductivity)

CBGW No.	Location name	Well type	Lat. (°N)	Long. (°E)	Depth bgl (m)	Fluoride (ppm)	EC (mS)
1	Gandhinagar	TW	23.24	72.68	54.9	1.6	0.5
2	Prantij	DCB	23.44	72.85	18.3	1.2	0.5
3	Prantij	TW	23.45	72.86	30.5	0.9	0.5
4	Shikha	DCB	23.39	73.23	30.5	0.4	0.6
5	Bayad	TW	23.22	73.21	18.3	0.9	4.8
6	Gundela	DW	23.12	73.36	9.1	1.3	0.8
7	Rojawa	TW	22.91	73.33	33.5	1.7	2.0
8	Lasundra	DW	22.91	73.14	6.1	3.4	7.4
9	Lasundra	DW	22.91	73.14	6.1	3.3	7.6
10	Sinhuj	DCB	22.82	72.86	24.4	2.4	2.3
11	Dakore	TW	22.76	73.16	36.6	4.3	2.4
12	Ladvel	HP	22.91	73.12	12.2	1.5	0.7
13	Kapadvanj	DCB	23.04	73.10	38.1	1.0	0.9
14	Kunha	TW	23.01	72.77	91.4	1.3	1.0
15	Lasundra	TW	22.92	73.15	85.3	1.1	2.0
16	Anghadi	DCB	22.81	73.30	24.4	0.6	0.7
17	Timba	HP	22.82	73.40	12.2	1.2	1.9
18	Tuwa	DW	22.80	73.46	0.9	3.4	3.4
19	Tuwa	DW	22.80	73.46	0.9	3.5	6.2
20	Tuwa	DW	22.80	73.46	0.9	3.3	6.2
21	Tuwa	HP	22.80	73.46	12.2	3.4	4.7
22	Tuwa	DW	22.80	73.46	6.1	0.8	0.7
23	Godhara	DW	22.78	73.60	7.3	0.8	0.8
24	Godhara	TW	22.76	73.61	30.5	0.8	0.5
25	Baska	HP	22.47	73.45	18.3	0.4	2.3
26	Baroda	TW	22.27	73.19	30.5	0.1	2.3
27	Jarod	HP	22.44	73.35	12.2	0.6	0.5
28	Khadki	HP	22.65	73.52	12.2	1.2	1.1
29	Dabhoi	HP	22.13	73.41	12.2	1.4	2.0
30	Sathod	TW	22.07	73.38	53.3	0.7	1.2
31	Sinor	TW	21.93	73.34	76.2	0.4	1.1
32	Adalaj	TW	23.17	72.58	228.6	0.8	2.1
33	Kalol	TW	23.26	72.47	182.9	0.6	2.3
34	Malharpur	HP	22.81	72.62	18.3	0.9	2.7
35	Marala	DCB	22.62	72.64	30.5	0.6	0.8
36	Khambhat	TW	22.33	72.62	91.4	0.8	2.8
37	Nadiad	TW	22.56	72.82	30.5	0.6	1.9
38	Bhadran	TW	22.37	72.90	67.1	1.3	2.2
39	Masar Rd.	TW	22.11	72.89	61.0	0.9	4.2

Table 4.2 continues

CBGW No.	Location name	Well type	Lat. (°N)	Long. (°E)	Depth bgl (m)	Fluoride (ppm)	EC (mS)
40	Kalak	DCB	22.02	72.76	21.3	1.1	2.2
41	Valu	HP	21.76	72.93	36.6	0.6	3.1
42	Baruch	TW	21.72	72.99	33.5	0.5	3.9
43	Manglej	TW	22.09	73.17	76.2	0.6	1.6
44	Dholka	TW	22.69	72.43	106.7	1.7	3.1
45	Dholera	TA	22.25	72.19	167.6	0.3	6.9
46	Bhavnagar	DW	21.80	72.07	12.2	3.4	59.6
47	Bhavnagar	TW	21.81	72.07	126.5	0.4	1.6
48	Bhavnagar	TW	21.81	72.07	228.6	0.7	2.9
49	Vallabhipur	TW	21.88	71.88	15.2	2.8	8.8
50	Rampara	TW	22.11	71.89	76.2	2.2	1.3
51	Dhandhuka	DCB	22.38	71.98	15.2	1.7	3.1
52	Bawala	TW	22.83	72.36	198.1	0.7	1.6
53	Bagodra	TA	22.64	72.20	335.3	0.3	1.9
54	Bagodra	TA	22.64	72.20	335.3	0.2	1.4
55	Gundi	TA	22.55	72.23	289.6	0.2	1.5
56	Batod	HP	22.16	71.66	36.6	0.5	1.0
57	Raliyana	TW	21.91	71.56	167.6	0.5	1.3
58	Vejalka	DCB	22.40	71.72	53.3	1.2	0.9
59	Wadhwan	TW	22.72	71.68	91.4	2.4	1.9
60	Bajana	TW	23.12	71.78	175.3	1.2	1.6
61	Dashada	TW	23.32	71.84	167.6	0.2	1.2
62	Sachana	TW	23.08	72.17	21.3	0.7	1.1
63	Vithalpur	TW	23.37	72.05	198.1	0.6	1.5
64	Umerkhaya	DW	22.90	72.02	12.8	9.9	7.6
65	Shiyala	TA	22.70	72.16	274.3	0.3	3.4
66	Ruhika	TA	22.66	72.23	457.2	0.2	3.0
67	Sarala	TA	22.67	72.20	274.3	0.2	2.6
68	Vithalgadh	DW	22.99	71.97	15.2	5.1	5.9
69	Nardipur	TW	23.25	72.56	199.6	0.8	1.2
70	Santej	TW	23.11	72.47	274.3	2.0	1.2
71	Rancharda	TW	23.08	72.45	213.4	0.9	1.1
72	Nardipur	TW	23.25	72.56	199.6	0.8	1.2
73	Santej	TW	23.11	72.47	274.3	2.0	1.2
74	Rancharda	TW	23.08	72.45	213.4	0.9	1.1
75	Ananddham	TW	22.99	72.52		1.8	2.1
76	Sarkhej	TW	22.99	72.49	91.4	2.0	1.9
77	Sarkhej	TW	22.99	72.49	18.3	2.0	2.2
78	Collet	TW	22.97	72.43	228.6	0.7	1.6
79	Collet	TW	22.98	72.44	61.0	2.4	3.6
80	Sanand	TW	23.00	72.38	228.6	1.6	3.2
81	Thol	TW	23.13	72.38	182.9	1.2	3.2
82	Thol	HP	23.15	72.37	24.4	1.3	3.2
83	Rangpurda	TW	23.25	72.30	182.9	1.3	2.3
84	Kadi	TW	23.30	72.31	213.4	2.0	1.6
85	Bhoyani Derasar	TW	23.36	72.23	243.8	0.6	2.4
86	Katosan Road	TW	23.40	72.24	243.8	1.2	2.9
87	Navdeep	TW	23.01	72.34	243.8	1.3	2.4
88	Vansa	DCB	23.02	72.33	12.2	1.6	1.4

Table 4.2 continues

CBGW No.	Location name	Well type	Lat. (°N)	Long. (°E)	Depth bgl (m)	Fluoride (ppm)	EC (mS)
89	Sachana	TW	23.08	72.16	213.4	0.3	1.7
90	Hansalpur	TW	23.10	72.07	109.7	2.7	2.3
91	Viramgam	TW	23.10	72.06	228.6	0.3	1.8
92	Juna Padhar	TW	23.19	72.04	243.8	0.2	1.6
93	Endla	TW	23.29	72.04	265.2	0.3	1.6
94	Sitapur	TW	23.45	71.99	182.9	0.6	1.8
95	Sitapur	TW	23.44	71.98	299.0	0.2	1.5
96	Valevda	TW	23.46	71.94	213.4	1.0	4.3
97	Valevda	TW	23.45	71.94	262.1	0.4	1.8
98	Dhanap	TW	23.26	72.75	213.4	1.4	1.0
99	Majara	TW	23.36	72.80	121.9	1.3	1.2
100	Talod	TW	23.35	72.93	45.7	0.5	1.3
101	Tajpur Camp	HP	23.37	73.03	24.4	2.1	1.6
102	Vadagam	HP	23.33	73.17	9.1	0.3	0.5
103	Ramnagar	HP	23.39	73.23	13.7	0.6	0.6
104	Dhamanya	HP	23.34	73.25	30.5	0.5	0.7
105	Kamaliya Kampa	HP	23.33	73.31	61.0	1.4	1.5
106	Ranmalgadh	TW	22.98	72.34	152.4	0.8	1.5
107	Rethal	TW	22.88	72.19	167.6	1.3	1.5
108	Shahpur	HP	22.88	72.02	18.3	7.1	8.5
109	Vasvelia	TW	23.00	72.04	167.6	0.2	2.3
110	Bhojva	TW	23.15	72.03	61.0	4.7	3.0
111	Malanpur	TW	23.25	71.93	274.3	0.6	2.0
112	Zainabad	TW	23.26	71.68	213.4	0.3	2.3
113	Zainabad	HP	23.26	71.68	14.9	3.9	0.9
114	Zinzuvada	TW	23.35	71.65	198.1	0.4	2.6
115	Zinzuvada	HP	23.35	71.66	15.2	0.9	0.7
116	Changodar	HP	22.93	72.44	9.1	2.7	1.7
117	Kalayangdh	TW	22.72	72.27	61.0	2.4	5.2
118	Limbdi	HP	22.57	71.81	13.7	5.0	3.4
119	Vadod	TW	22.56	71.63	53.3	1.1	1.5
120	Zinzawadar	TW	22.45	71.69	285.0	0.8	3.5
121	Zinzawadar	HP	22.45	71.69	45.7	0.4	1.3
122	Chuda	TW	22.49	71.69	182.9	1.2	3.9
123	Vekaria	HP	22.82	72.06	12.2	5.0	6.6
124	Fulgam Jn	HP	22.54	71.54	54.9	0.9	1.1
125	Shekhpur	TW	22.70	71.56	54.9	2.3	5.3
126	Vana	HP	22.87	71.71	12.2	8.4	6.0
127	Rangpur	DW	22.41	71.93	10.7	1.3	9.0
128	Vagad	DW	22.36	71.87	18.3	1.8	3.7
129	Nagnesh	TW	22.36	71.76	61.0	1.2	2.2
130	Nagnesh	HP	22.36	71.76	38.1	2.2	2.3
131	Alampur	DW	22.30	71.66	16.8	0.7	0.6
132	Paliyad	HP	22.25	71.56	45.7	0.7	2.3
133	Paliyad	TW	22.25	71.56	91.4	0.6	1.4
134	Botad	HP	22.17	71.66	48.8	0.6	0.9
135	Tatam	TW	22.06	71.62	64.0	4.6	1.1
136	Gadhda	TW	21.96	71.58	61.0	0.5	2.2
137	Ahmedabad	TW	22.98	72.62	233.2	1.3	1.5
138	Hathijan	TW	22.94	72.64	137.2	1.8	1.1

Table 4.2 continues

CBGW No.	Location name	Well type	Lat. (°N)	Long. (°E)	Depth bgl (m)	Fluoride (ppm)	EC (mS)
139	Onthwari	DCB	22.82	72.80	61.0	1.7	2.0
140	Ran Na Muvada	DCB	22.84	72.95	85.3	1.0	1.5
141	Porda	DCB	22.92	73.00	67.1	1.4	0.8
142	Dhasa	TW	21.80	71.51	91.4	0.3	1.7
143	Mandva	HP	21.81	71.58	36.6	0.7	0.8
144	Dedakdi	TW	21.81	71.71	57.9	0.8	2.1
145	Umrالا	HP	21.84	71.80	45.7	1.4	1.0
146	Kanpar	TW	21.96	71.88	21.3	5.9	2.4
147	Sarangpur	HP	22.16	71.77	61.0	0.7	2.2
148	Navagam	TW	21.96	71.90	61.0	2.9	3.2
149	Panavi	TW	22.08	71.89	125.3	0.4	6.0
150	Keriya Dhal	TW	22.11	71.89	182.9	2.5	0.8
151	Vaya	DW	22.20	71.87	30.5	3.8	1.0
152	Devthal	DCB	22.75	72.13	9.8	3.1	9.6
153	Devthal	TW	22.76	72.12	274.3	0.3	2.6
154	Kanera	TW	22.81	72.62	137.2	2.6	3.2
155	Sokhada	TW	22.74	72.68	97.5	1.6	5.7
156	Matar	TW	22.71	72.68	109.7	3.9	0.9
157	Nar	TW	22.48	72.71	106.7	0.5	2.5
158	Jogan	DCB	22.45	72.79	33.5	3.5	0.9
159	Bharel	TW	22.41	72.83	61.0	0.9	0.9
160	Dededa	DW	22.46	72.91	57.9	0.8	1.4
161	Anand	TW	22.53	72.96	45.7	0.6	0.8
162	Uttarsanda	TW	22.66	72.90	54.9	1.2	1.2
163	Sojitra	TW	22.55	72.74	140.2	0.7	1.5
164	Jedwapura	TW	22.55	72.83	91.4	0.7	2.3
165	Bedva	DCB	22.55	73.04	36.6	0.4	0.8
166	Ode	TW	22.62	73.11	47.2	0.6	0.8
167	Lingda	HP	22.69	73.08	19.8	1.5	0.7
168	Alindra	HP	22.70	72.97	54.9	0.6	0.6
169	Vaghasi	TW	22.54	73.00	48.8	1.2	0.9
170	Bhetasi	TW	22.43	73.02	61.0	1.0	1.2
171	Samiala	TW	22.26	73.12	112.8	0.8	0.9
172	Dabhasa	TW	22.25	73.05	76.2	0.7	1.0
173	Vadu	DCB	22.21	72.98	51.2	0.6	1.4
174	Vadu	TW	22.22	72.98	130.5	0.8	2.1
175	Gavasadj	TW	22.19	72.97	129.5	0.7	0.9
176	Jambusar	TW	22.05	72.81	73.2	0.9	3.4
177	Nahiyer	TW	21.96	72.88	61.0	0.5	3.9
178	Haldarva	TW	21.89	73.07	70.1	0.4	2.4
179	Karjan	TW	22.05	73.12	106.7	0.5	2.0
180	Saring	DCB	21.89	73.12	36.6	0.4	1.7
181	Arjanpura	DCB	21.87	73.16	48.8	0.4	1.4
182	Garudeshwar	TW	21.89	73.66	88.4	1.4	0.8
183	Garudeshwar	TW	21.89	73.66	64.0	1.3	0.7
184	Kanara	TW	22.08	73.40	182.9	0.6	1.0
185	Mandwa	TW	22.01	73.43	45.7	0.4	0.7
186	Chandod	TW	22.99	73.46	121.9	0.3	0.8
187	Ankhi	TW	22.13	73.20	91.4	0.5	2.4
188	Kayvarohan	TW	22.08	73.24	99.1	0.3	1.2

Table 4.2 continues

CBGW No.	Location name	Well type	Lat. (°N)	Long. (°E)	Depth bgl (m)	Fluoride (ppm)	EC (mS)
189	Dantiwada	HP	24.17	72.48	36	0.3	0.5
190	Dantiwada	TW	24.16	72.48	100.6	0.8	0.6
191	Gola	DCB	24.19	72.78	36.6	0.4	0.7
192	Dharoi	HP	24.00	72.85	12.2	1.6	0.6
193	Mumanvas	DW	24.04	72.83	18.3	1.5	0.9
194	Mathasur	HP	23.80	73.01	45.7	1.6	1.2
195	Himmatnagar	HP	23.72	72.96	27.4	1.6	0.9
196	Dalpur	DCB	23.51	72.95	21.3	0.2	0.6
202	Math	HP	23.43	73.82	15.2	0.6	0.4
203	Aritha	HP	23.14	73.65	15.2	0.8	0.5
204	Limbodra	HP	23.19	73.60	15.2	0.8	0.7
205	Ghaliya Danti	HP	23.36	73.51	18.3	0.8	0.8
206	Shehra	HP	22.95	73.63	18.3	1.1	0.5
207	Popatpura	HP	22.79	73.45	18.3	1.3	0.6
208	Maniyor	TW	23.82	72.96	73.9	3.1	1.9
209	Dharewada	TW	23.98	72.39	212.3	0.2	3.5
210	Ganguva	TW	24.16	72.73	85.5	0.7	0.5
211	Chadotar	TW	24.21	72.39	63.4	0.9	1.0
212	Bhadath	TW	24.34	72.20	140.9	1.1	0.4
213	Kuwarava	TW	24.04	71.90	186.6	1.9	1.7
214	Kuwarava	TW	24.05	71.90	121.9	1.9	0.0
215	Tharad	TW	24.41	71.64	299.1	0.8	3.4
216	Jitoda	TW	23.74	72.15	312.7	2.0	2.3
217	Jitoda	TW	23.74	72.15	426.7	1.0	0.0
218	Sami	TW	23.70	71.78	298.7	0.4	3.9
219	Wavadi	TW	23.92	72.52	144.9	1.6	1.0
220	Pilwai	TW	23.53	72.69	235.4	0.6	1.6
221	Pilwai	TW	23.54	72.68	152.4	0.7	1.3
222	Heduva	TW	23.57	72.34	266.7	0.8	2.3
223	Vaghpur	TW	23.68	73.42	85.8	1.0	1.4
224	Edla	TW	23.54	72.06	288.7	0.7	2.6
225	Sherisa	TW	23.20	72.48	232.3	1.1	1.7
312	Diyodar	TW	24.10	71.74	207.3	0.7	1.8
313	Diyodar	TW	24.10	71.74	207.3	0.6	4.1
314	Tharad	TW	24.41	71.64	201.2	0.3	2.4
316	Agathala	TW	24.29	71.88	137.2	1.0	1.8
317	Sujanipur	TW	23.89	72.11	91.4	2.0	9.5
318	Sujanipur	TW	23.90	72.12	326.1	0.9	3.6
319	Sujanipur	TW	23.91	72.12	39.6	3.1	5.3
320	Kuwarva	TW	24.04	71.90	186.6	1.7	1.9
321	Kharia	TW	23.94	71.83	158.5	2.3	1.0
322	Sami	TW	23.70	71.78	298.7	0.3	4.7
323	Hedva	TW	23.57	72.34	82.3	0.8	3.1
324	Kuder	TW	23.70	71.87	262.1	2.9	2.5
325	Patan	TW	23.84	72.11	198.1	3.1	2.0
326	Patan	TW	23.84	72.11	129.5	3.5	1.8
327	Patan	TW	23.84	72.11	60.0	2.1	3.4
328	Jitoda	TW	23.74	72.15	312.7	1.6	3.3

Table 4.2 continues

CBGW No.	Location name	Well type	Lat. (°N)	Long. (°E)	Depth bgl (m)	Fluoride (ppm)	EC (mS)
329	Jitoda	TW	23.74	72.15	448.1	0.7	4.3
330	Kamboi	TW	23.67	72.02	213.4	1.2	2.8
331	Muthia	TW	23.09	72.69	141.7	1.7	1.4
332	Paliya	TW	23.18	72.83	118.9	0.8	1.6
333	Punsari	TW	23.39	73.10	32.3	0.6	0.7
334	Dalani Muwadi	TW	23.36	72.88	91.4	0.8	1.6
335	Rojad	HP	23.35	73.09	28.7	0.6	1.7
336	Vadrad	TW	23.42	72.89	57.9	1.4	1.6
337	Tejpur	TW	23.39	72.81	160.0	0.7	1.7
338	Navalpur	TW	23.60	72.90	121.9	0.8	1.5
339	Dhanap	TW	23.26	72.75	167.6	1.3	1.7
340	Indroda Park	TW	23.19	72.65	106.7	1.0	1.2
341	Rupawati	TW	23.00	72.30	213.4	0.8	2.1
342	Sokali	TW	23.10	72.11	93.0	2.0	4.6
343	Dulapur	TW	23.02	71.58	61.0	1.8	3.5
355	Salajada	TW	22.80	72.39	168.0	0.6	2.3
356	Salajada	TW	22.79	72.39	198.4	0.6	2.3
357	Salajada	TW	22.79	72.39	93.0	1.6	4.9
358	Gundi	TA	22.55	72.23	289.6	0.3	4.1
359	Shiyal	TW	22.68	72.16	274.3	0.2	4.6
360	Padgol	TW	22.59	72.84	137.2	0.4	1.8
361	Morad	TW	22.54	72.86	91.4	0.3	1.2
362	Gumadia	TW	22.76	73.23	48.8	0.7	1.3
363	Kund-9	TS	22.80	73.46	1.0	3.0	7.2
364	Kund-13	TS	22.80	73.46	1.0	3.2	7.4
365	Kund-20	TS	22.80	73.46	1.0	3.1	7.1
366	Kund-28	TS	22.80	73.46	1.0	3.5	8.0
367	Dholera	TA	22.25	72.19	168.0	0.3	7.2

It is seen (Figure 4.5) that pockets of high groundwater fluoride concentration in NGC region are approximately aligned around four linear belts marked PP', QQ', RR' and SS'. The pockets of very high fluoride concentration values (4 to 8 ppm) are aligned around PP' linking LRK-NS-GC, roughly in the North-South direction. To the east of PP', there is another linear belt around QQ' within the Cambay Basin with patches of high fluoride concentration values (1.5 to 4 ppm). On the eastern most part lies the linear belt around RR', almost in the recharge area in the Aravalli foothills and is roughly parallel to it, with several small and isolated pockets of fluoride concentration >1.5 ppm. The fourth linear belt of high fluoride concentration (4 to 8 ppm) is around SS', roughly in the East-West direction, linking the region of thermal springs of Tuwa and Lasundra in the east to the Nalsarovar in the west.

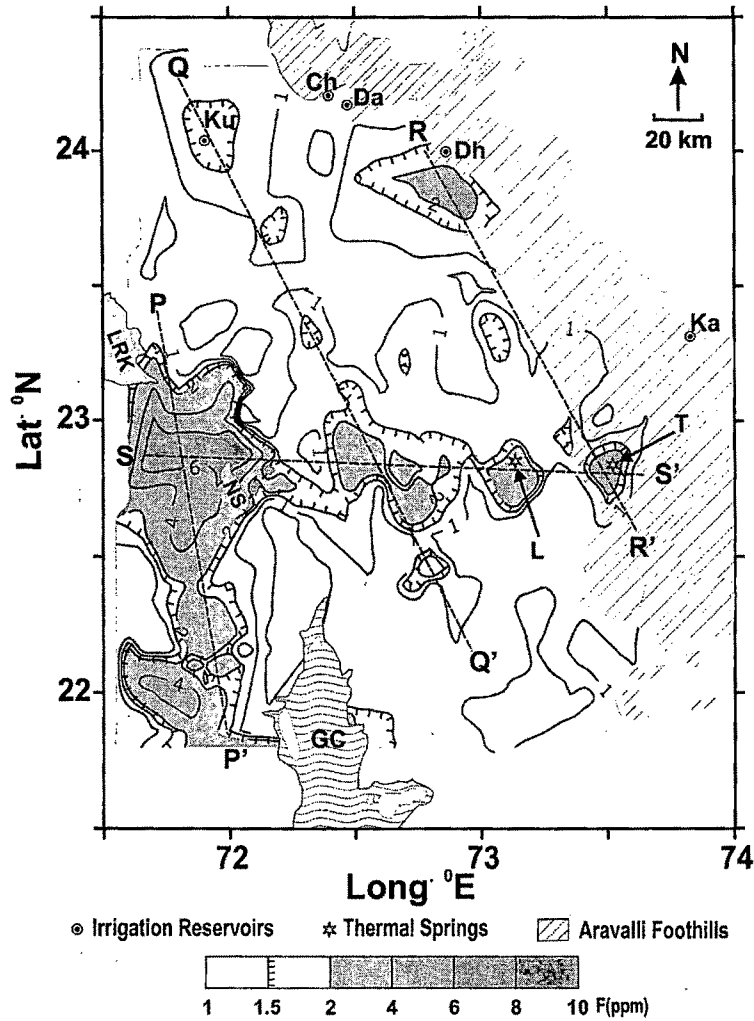


Figure 4.5 Isoline map of the fluoride concentration in groundwater – NGC region. Patches of high fluoride concentration (>1.5 ppm) appear to be aligned around four lines (PP', QQ', RR' and SS') separated by areas with low fluoride. Acronyms: Ch –Chadotar; Ku –Kuwarva; Da –Dantiwada; Dh –Dharoi; Ka –Kadana; L –Lasundra; T –Tuwa.

Figure 4.6(a) shows depth below ground level (bgl) of the sampled wells vs. fluoride concentration in groundwater in the NGC region. Very high fluoride concentrations are found even in shallow (depth <20 m) wells in some locations and low concentrations are found in very deep (depth >300 m) wells in other locations in the region. In some other locations inverse relationship is also observed. A similar plot using the same dataset but only taking samples with fluoride concentration >1.5 ppm is shown in Figure 4.6(b). Samples belonging to aquifers from different parts of the study area, namely, (i) along LRK-NS-GC tract, (ii) on the flanks of the Cambay Basin, and (iii) within Cambay Basin, are also identified in Figure 4.6(b).

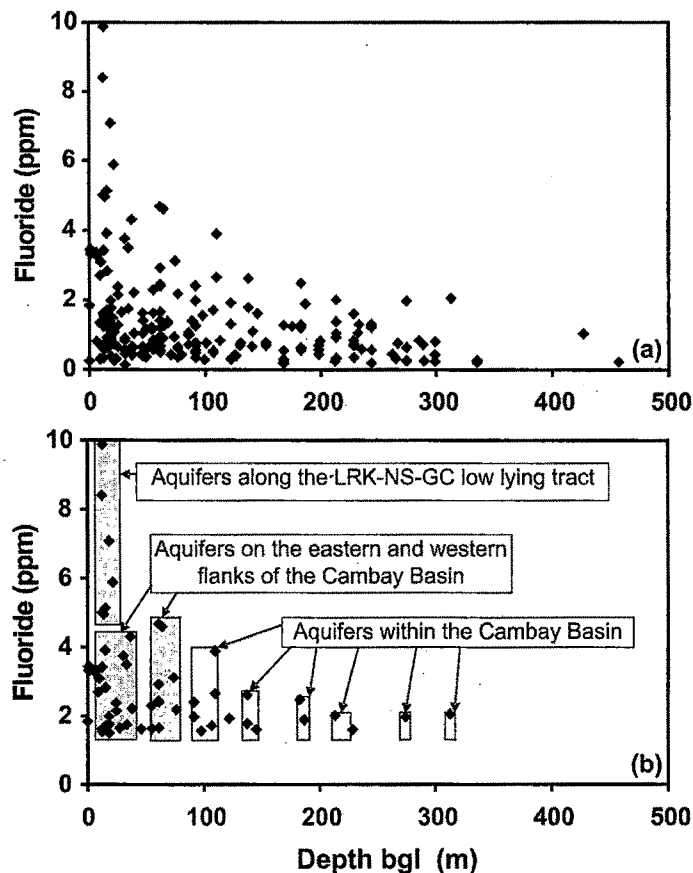


Figure 4.6 (a) Depth of sampled wells (bgl) vs. fluoride concentration for all sampled wells. (b) Samples with fluoride concentration <1.5 ppm area removed from plot (a). Several aquifer depth zones with >1.5ppm groundwater fluoride are identified within the Cambay basin.

Most fluoride-rich ground waters from the depth zone up to 40 m occur on the west flank of Cambay Basin where aquifers comprise either fluvio-marine sediments deposited in the LRK-NS-GC tract or Mesozoic sandstones farther west. Tubewells shallower than ~40 m and showing fluoride concentration <1.5 ppm are mainly located on the east flank of Cambay Basin. Tubewells tapping the depth zones of 53-76 m and yielding groundwater with fluoride concentration >1.5 ppm are located on both east and west flanks of the Cambay Basin. All fluoride rich tubewells with depth ranging from 90 m to ~310 m are located within the Cambay Basin. It is also noted that in the Cambay Basin fluoride rich groundwater is limited only to certain depth zones. It is possible, to identify six fluoride rich sub-aquifer depth zones (Table 4.3) within the Cambay Basin.

Table 4.3 Sub-aquifer depth zones having high fluoride in the Cambay Basin.

Zone	Depth range (m)	Zone	Depth range (m)
I	90-110	IV	210-230
II	135-145	V	~275
III	180-190	VI	~310

Identifying these fluoride rich sub-aquifer depth zones, based on groundwater fluoride concentration in samples across a large area within Cambay Basin, has an inherent assumption of the continuity of these sub-aquifers at approximately the same depth (bgl) throughout the Cambay Basin. This assumption seems reasonable considering the subsurface lithological cross-section (Figure 1.6), wherein it is seen that at a particular depth (bgl) generally the same sub-aquifer is encountered at different locations along the profile within the Cambay Basin. This is also seen in several other cross sections drawn across the Cambay Basin by the GWRDC (unpublished data). It seemed possible that if these fluoride rich sub-aquifers are tapped by a particular tubewell (which may also be tapping other sub-aquifers), the fluoride concentration in the overall groundwater pumped from this tubewell may be relatively higher.

To verify the above possibility, a tubewell (marked A in Figure 4.7) in Chadotar village outside the Cambay Basin and four other tubewells in the vicinity of each other (marked B to E) in Kuwarva village (~50 km away from Chadotar) within the Cambay Basin were examined for any correlation between fluoride content in groundwater from these tubewells and fluoride rich sub-aquifers tapped (see Figure 4.5 for locations of these villages). The fluoride concentration in groundwater from these tubewells, the depth (bgl) of sampled well and the fluoride rich sub-aquifer depth zones (see Table 4.3) tapped by these tubewells are shown in Figure 4.7. It is seen that the shallowest (63 m) Tubewell – A at Chadotar does not tap any of the fluoride rich sub-aquifers and has a low fluoride content of 0.9 ppm. The Tubewell-B, tapping fluoride rich sub-aquifer Zone-I and Zone-II, has the highest fluoride concentration of 2.2 ppm. Tubewell – C taps only fluoride rich sub-aquifer Zone-I and its fluoride content is 1.9 ppm. Tubewell – D tapping three fluoride rich sub-aquifer Zones (I, II and III) has groundwater fluoride concentration of 1.9 ppm. The deepest Tubewell-E (185 m) tapping only a small part of fluoride rich zone-I and two other fluoride rich Zones (II and III) has fluoride content of 1.5 ppm. It is thus seen that Tubewell (A), not tapping any of the high fluoride sub-aquifers has the lowest fluoride content. Tubewells tapping any of the fluoride rich sub-aquifer depth zones, in general, have higher fluoride content.

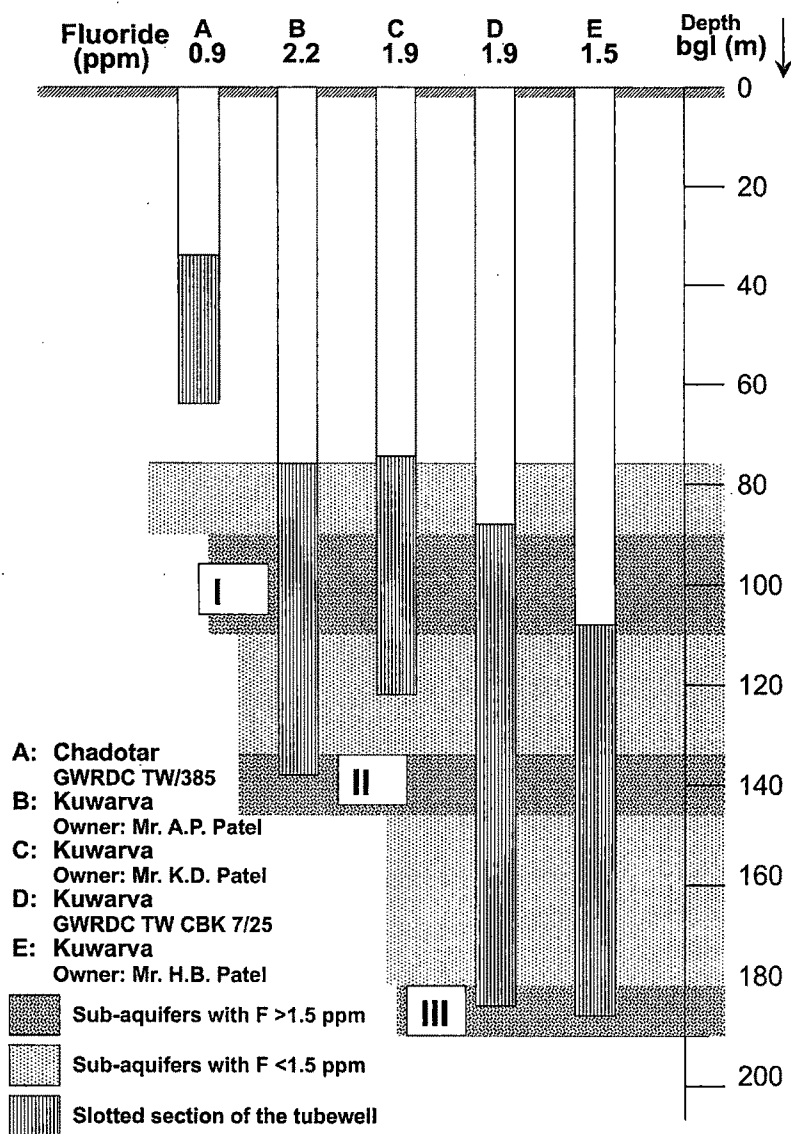


Figure 4.7 A comparison of groundwater fluoride content and fluoride rich sub-aquifer depth zones tapped in selected five tubewells. The shallowest tubewell–A does not tap any of the fluoride rich sub-aquifer depth zones and has the lowest fluoride content in groundwater. Tubewell–B, tapping zones I and II, has the highest fluoride in groundwater. The deepest tubewell E, which taps sub-aquifers from depth zones –II and –III but does not tap zone–I, has comparatively lower fluoride content of 1.5 ppm.

However, due to limited number of available tubewells providing suitable conditions (such as at Chadotar and Kuwarva) for verification, the possibility that certain depth zones in the Cambay Basin largely contribute groundwater rich in fluoride, could not be substantiated further in the present study.

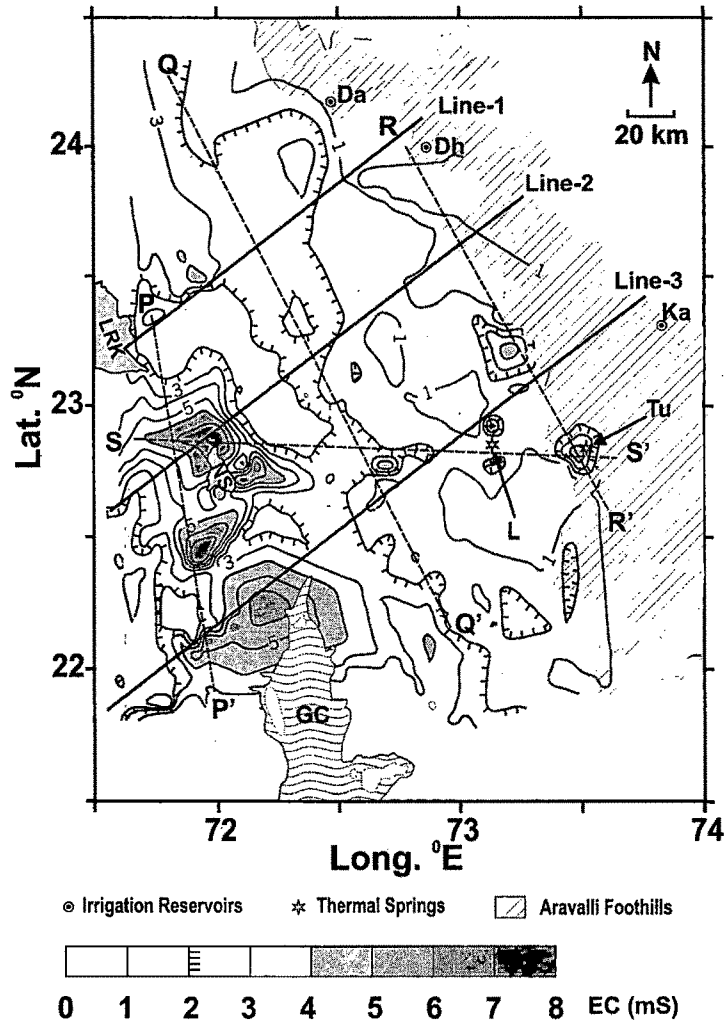


Figure 4.8 Isoline map of EC of groundwater from study area. Areas of high EC overlap in general with areas of high fluoride shown in Fig. 4.5. Acronyms for the locations are: Da –Dantiwada; Dh –Dharoi; Ka –Kadana; L –Lasundra; T –Tuwa. The geographical covariation of EC and fluoride along Lines 1-3 and SS' is shown in Figure 4.9

4.1.3 Groundwater Electrical Conductivity

An isoline map of Electrical Conductivity (EC) of groundwater samples from the NGC region is shown in Figure 4.8 . Details of sampling locations and values of EC are given in Table 4.2. The EC values range from 0.3 to 8 mS, with values >5 mS in the LRK-NS-GC belt and the lowest values in isolated pockets along the Aravalli foothills. In general, areas with high EC overlap with those having high fluoride concentration (Figure 4.5). However, a pocket of high EC (>3 mS) in the NW part of the study area has low fluoride concentration (<1.5 ppm). Another pocket of EC ~1 mS, around 24°N in the Aravalli foothills, on the other hand, has high fluoride concentration (>1.5 ppm). In spite of these differences, it can be seen from Figure 4.8 that high EC regions are

approximately aligned around the same lines PP', QQ', RR', SS' that show high fluoride concentrations around them. The central (QQ') belt of both high fluoride concentration and EC is flanked on either side by belts of relatively lower values.

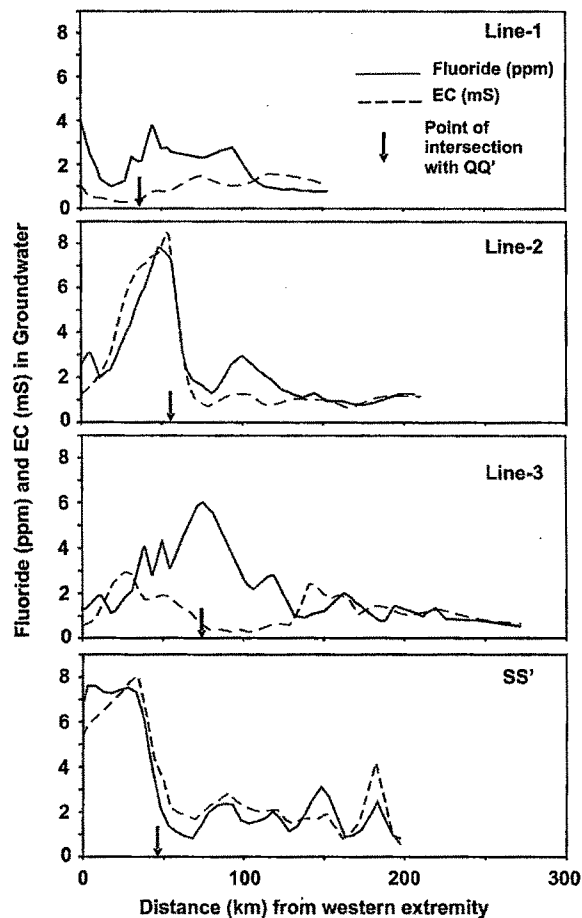


Figure 4.9 Geographical co-variation of fluoride and EC of groundwater along the four lines (1, 2, 3 and SS' in Figure 4.8) in NGC region. Distances are measured from the western end of each line and the arrow marks the point of intersection of each of these lines with QQ'. It is seen that the two parameters co-vary in the Cambay basin and the central belt of high fluoride – high EC is flanked by relatively lower values on either side.

With a view to observe the geographical co-variation of EC and fluoride concentration more clearly, their variation along four lines (Line-1, Line-2, Line-3 and the line SS' in Figure 4.8) is shown in Figure 4.9. The EC and fluoride concentrations at a particular point are plotted against the distance of that point from the western end of respective lines. Since these four lines intersect the line QQ', the point of intersection of these lines with QQ' is used as a reference point and marked in Figure 4.9 to compare the relative variation in EC and fluoride at a particular distance along these lines.

Whereas the two parameters appear to generally co-vary, a westward displacement of the high EC region relative to high fluoride region is seen along the Line-3.

Although geographical coincidence of areas having high fluoride concentrations with those having high EC in groundwater is visible from Figure 4.5 and Figure 4.8, no statistical correlation between these two is seen in the scatter plot (Figure 4.10) for the entire NGC region.

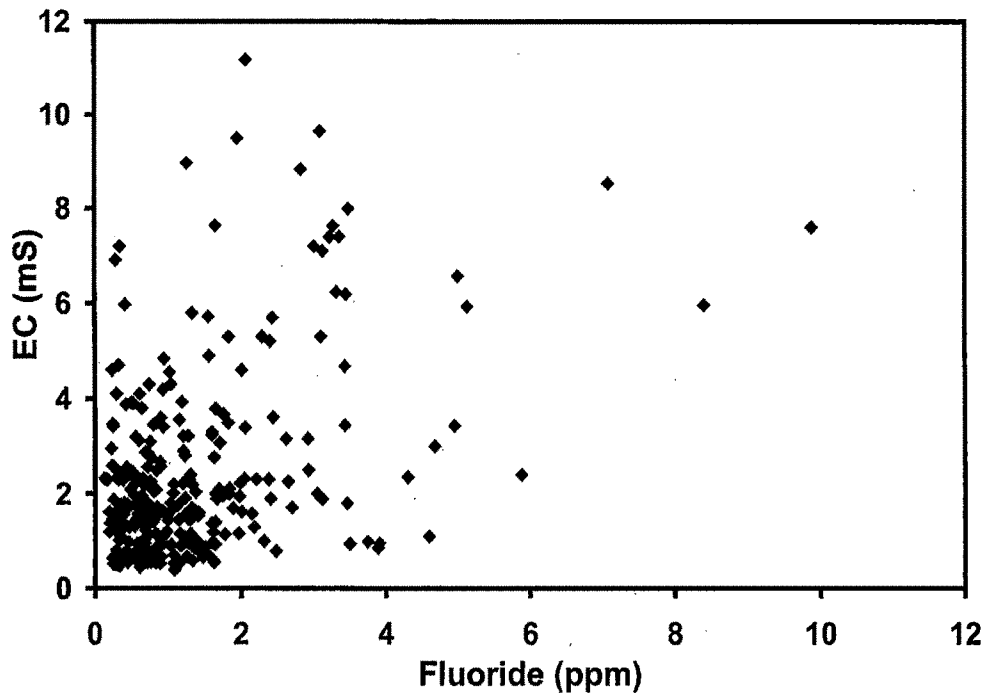


Figure 4.10 A scatter plot of fluoride concentration vs. EC in groundwater from the NGC region, showing absence of correlation between the two.

4.1.4 Fluoride and EC in Modern Precipitation

With a view to have an idea about ionic concentration in modern precipitation, dissolved fluoride and EC were measured in fortnightly accumulated precipitation samples collected at six dam sites (Dantiwada, Dharoi, Kadana, Shetrunji, Bhadar and Ukai; see Figure 4.14) located in and around the NGC region. The variation in rainfall, fluoride and EC in each fortnightly accumulated precipitation samples is shown in Figure 4.11 (for Dantiwada, Dharoi and Kadana) and Figure 4.12 (for Bhadar, Shetrunji and Ukai). It is seen that variations in both fluoride concentration and EC of successive fortnightly accumulated precipitation samples are nearly proportional, except for Ukai. The slopes (Figure 4.13) and intercepts of the best fit lines are, however, location dependent. It is also seen from Figure 4.11 and Figure 4.12 that variations in fluoride and EC are not

related to variation in the local rainfall amount. Samples with relatively higher fortnightly rainfall do not necessarily have relatively lower fluoride and EC and vice versa. Precipitation samples from Dantiwada and Dharoi, located in the semi- arid parts of NGC region, have a distinctly higher range of fluoride and EC compared to other locations which are relatively less arid.

The highest and the average fluoride content at these stations as well as their relative latitudinal positions with reference to NGC region are shown in Figure 4.14. It is seen that Dantiwada, with highest aridity amongst these stations, has the highest fluoride levels in precipitation. The range, the highest value and the seasonal average of both fluoride and EC in precipitation from NGC region decreases with decreasing aridity southwards (see Figure 4.11 and Figure 4.12).

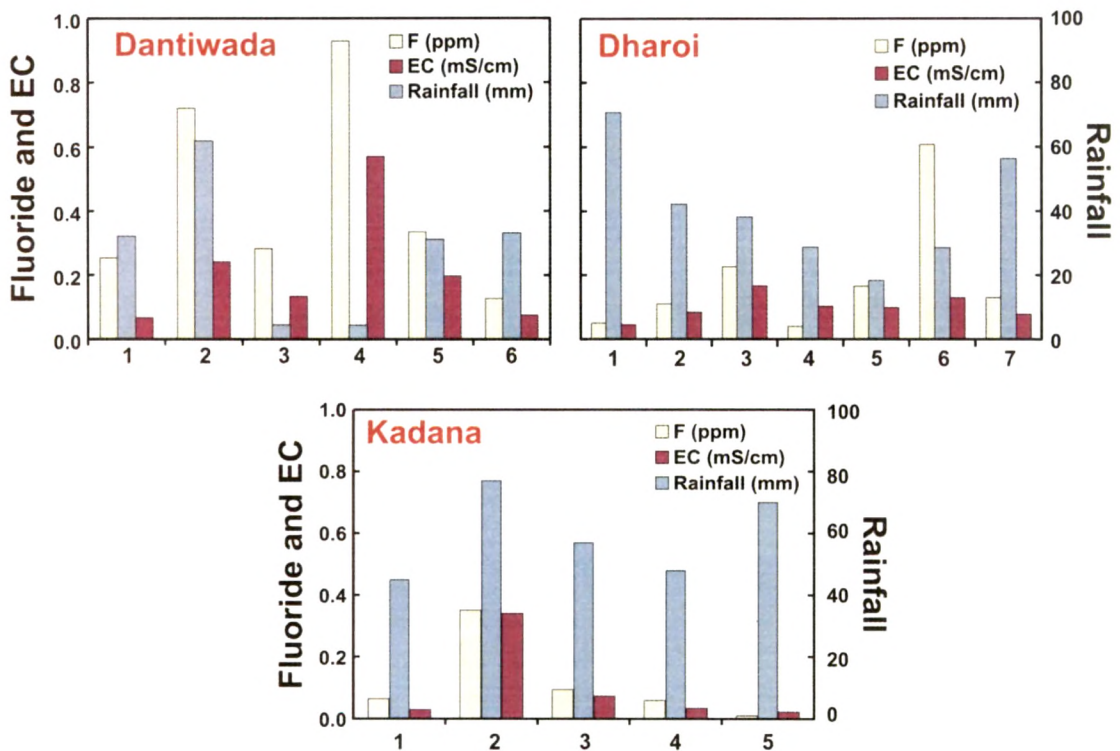


Figure 4.11 Variation in the amount of rainfall, dissolved fluoride and EC in the fortnightly accumulated precipitation samples at the dam sites of Dantiwada, Dharoi and Kadana. The locations of these dam sites within NGC region are shown in Figure 4.8.

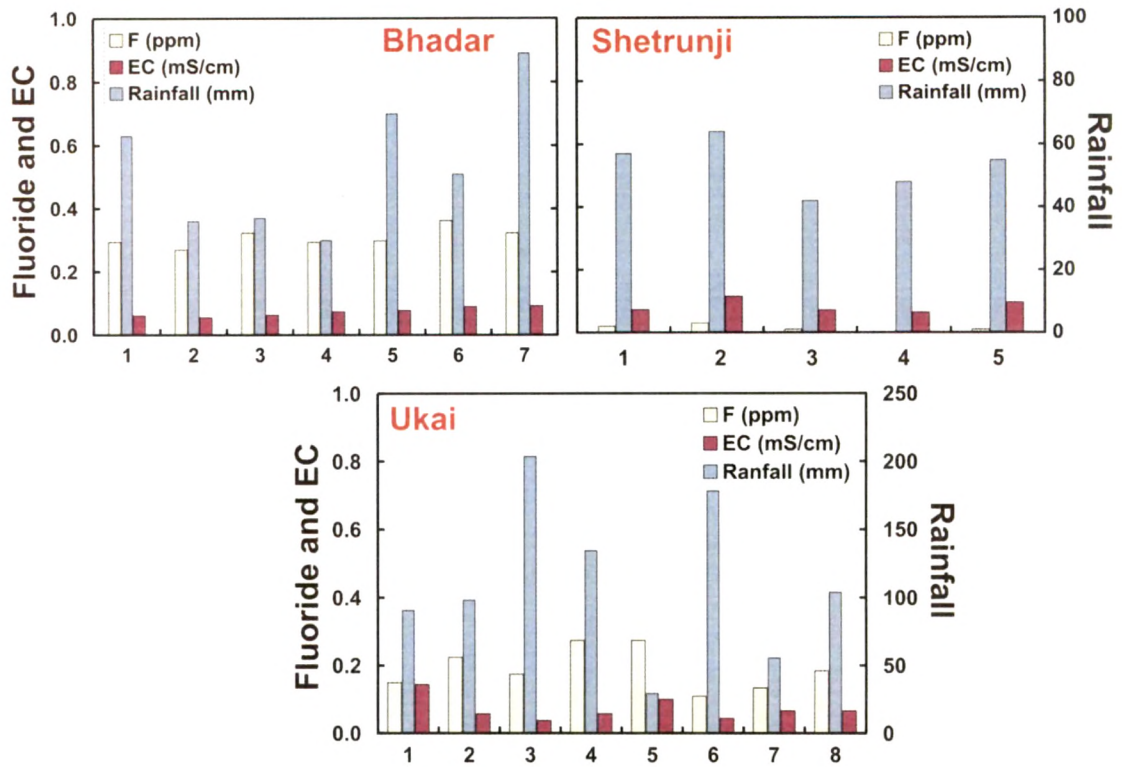


Figure 4.12 Variation in the amount of rainfall, dissolved fluoride and EC in the fortnightly accumulated precipitation samples at the dam sites of Bhadar, Shetrunji and Ukai. The locations of these dam sites are shown in Figure 4.14.

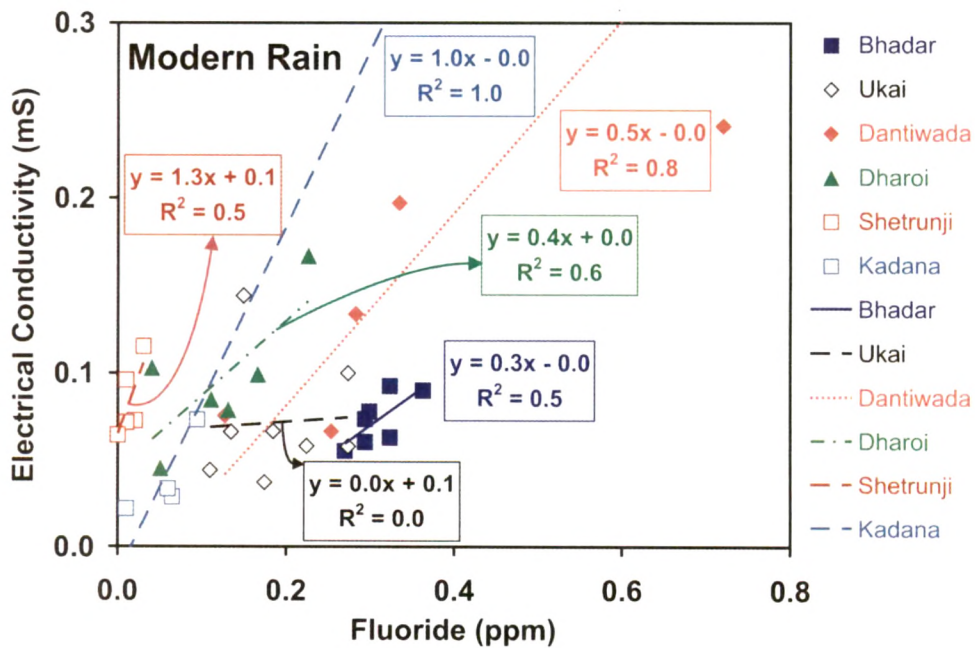


Figure 4.13 Relationship between dissolved fluoride and EC in modern rainwater collected at the six dam sites in and around NGC region.

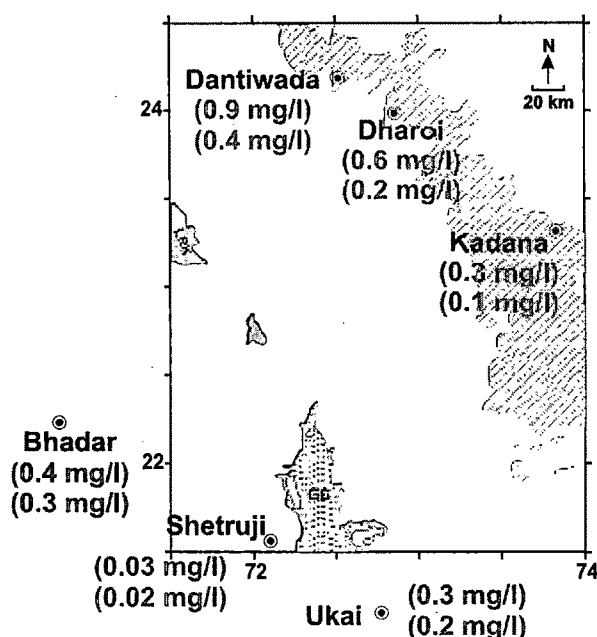


Figure 4.14 The highest and the average fluoride content at various dam sites and their relative latitudinal positions with reference to the NGC region.

4.1.5 Stable Isotopes of Oxygen and Hydrogen

Details of the (i) sampled well locations; (ii) location names; (iii) well type; (iv) measured values $\delta^{18}\text{O}$, δD ; and the (v) calculated values of *d*-excess for groundwater from NGC region are given in Table 4.4. Similar details for precipitation samples are given in Table 4.5. Plots of $\delta^{18}\text{O}$ vs. δD , and $\delta^{18}\text{O}$ vs. *d*-excess for ground water and fortnightly precipitation samples from NGC region are shown in Figure 4.15.

Table 4.4 Details of groundwater sampling sites together with measured values of $\delta^{18}\text{O}$, δD and *d*-excess in the NGC region. (TW = tubewell; DCB= dug cum bore; DW = dug well; HP = hand pump; TA = thermal artesian; TS = thermal spring; bgl = below ground level; CBGW = Cambay Basin Ground Water)

CBGW Sample No.	Location name	Well type	Lat. (°N)	Long. (°E)	Depth bgl (m)	$\delta^{18}\text{O}$ (‰)	δD (‰)	<i>d</i> -excess (‰)
9	Lasundra	DW	22.91	73.14	6.1	-1.08	-17.5	-8.9
15	Lasundra	TW	22.92	73.15	85.3	-1.80	-18.3	-3.9
32	Adalaj	TW	23.17	72.58	228.6	-2.96	-26.4	-2.7
40	Kalak	DCB	22.02	72.76	21.3	-1.67	-15.0	-1.7
43	Manglej	TW	22.09	73.17	76.2	-1.68	-13.0	0.5
45	Dholera	TA	22.25	72.19	167.6	-1.96	-26.8	-11.1

Table 4.4 continues

CBGW Sample No.	Location name	Well type	Lat. (°N)	Long. (°E)	Depth bgl (m)	$\delta^{18}\text{O}$ (‰)	δD (‰)	d-excess (‰)
53	Bagodra	TA	22.64	72.20	335.3	-0.77	-24.6	-18.4
55	Gundi	TA	22.55	72.23	289.6	-2.97	-26.1	-2.3
56	Batod	HP	22.16	71.66	36.6	-1.61	-19.6	-6.8
58	Vejalka	DCB	22.40	71.72	53.3	-1.35	-16.6	-5.8
65	Shiyala	TA	22.70	72.16	274.3	-1.97	-24.4	-8.6
66	Ruhika	TA	22.66	72.23	457.2	-2.36	-25.8	-6.9
67	Sarala	TA	22.67	72.20	274.3	-1.91	-25.6	-10.3
76	Sarkhej	TW	22.99	72.49	91.4	-3.08	-25.3	-0.7
89	Sachana	TW	23.08	72.16	213.4	-2.08	-23.9	-7.3
98	Dhanap	TW	23.26	72.75	213.4	-3.14	-26.8	-1.7
99	Majara	TW	23.36	72.80	121.9	-2.69	-23.9	-2.4
100	Talod	TW	23.35	72.93	45.7	-2.92	-24.1	-0.8
102	Vadagam	HP	23.33	73.17	9.1	-2.26	-23.0	-5.0
104	Dhamanya	HP	23.34	73.25	30.5	-2.34	-22.4	-3.7
109	Vasvelia	TW	23.00	72.04	167.6	-3.31	-26.2	0.2
112	Zainabad	TW	23.26	71.68	213.4	-3.52	-26.5	1.7
114	Zinzuvada	TW	23.35	71.65	198.1	-3.15	-16.7	8.5
115	Zinzuvada	HP	23.35	71.66	15.2	-0.45	-14.9	-11.3
120	Zinzawadar	TW	22.45	71.69	285.0	-3.06	-26.6	-2.2
122	Chuda	TW	22.49	71.69	182.9	-0.73	-20.0	-14.1
124	Fulgam Jn	HP	22.54	71.54	54.9	-2.35	-21.7	-2.9
125	Shekhpur	TW	22.70	71.56	54.9	-0.88	-20.7	-13.7
126	Vana	HP	22.87	71.71	12.2	-1.42	-19.6	-8.2
132	Paliyad	HP	22.25	71.56	45.7	-0.38	-13.0	-9.9
135	Tatam	TW	22.06	71.62	64.0	-1.66	-19.1	-5.8
141	Porda	DCB	22.92	73.00	67.1	-2.89	-23.1	0.0
147	Sarangpur	HP	22.16	71.77	61.0	-0.51	-11.2	-7.2
149	Panavi	TW	22.08	71.89	125.3	-2.38	-23.1	-4.0
151	Vaya	DW	22.20	71.87	30.5	-2.19	-18.4	-0.9
153	Devthal	TW	22.76	72.12	274.3	-2.59	-26.0	-5.3
155	Sokhada	TW	22.74	72.68	97.5	-2.68	-21.6	-0.1
159	Bharel	TW	22.41	72.83	61.0	-1.65	-18.3	-5.1
161	Anand	TW	22.53	72.96	45.7	-2.44	-21.6	-2.1
179	Karjan	TW	22.05	73.12	106.7	-1.50	-15.5	-3.5
185	Mandwa	TW	22.01	73.43	45.7	-2.00	-13.5	2.5
186	Chandod	TW	22.99	73.46	121.9	-2.10	-16.3	0.5
208	Maniyor	TW	23.82	72.96	73.9	-3.25	-21.6	4.4
209	Dharewada	TW	23.98	72.39	212.3	-3.94	-27.9	3.7
210	Ganguva	TW	24.16	72.73	85.5	-3.42	-28.9	-1.5
211	Chadotar	TW	24.21	72.39	63.4	-1.99	-29.9	-14.1
213	Kuwarva	TW	24.04	71.90	186.6	-4.08	-30.1	2.5
214	Kuwarva	TW	24.05	71.90	121.9	-2.84	-30.1	-7.3
215	Tharad	TW	24.41	71.64	299.1	-2.72	-28.2	-6.5

Table 4.4 continues

CBGW Sample No.	Location name	Well type	Lat. (°N)	Long. (°E)	Depth bgl (m)	$\delta^{18}\text{O}$ (‰)	δD (‰)	d-excess (‰)
216	Jitoda	TW	23.74	72.15	312.7	-1.38	-22.3	-11.3
218	Sami	TW	23.70	71.78	298.7	-3.16	-26.2	-1.0
220	Pilwai	TW	23.53	72.69	235.4	-3.16	-23.7	1.6
223	Vaghpur	TW	23.68	73.42	85.8	-3.30	-25.9	0.5
224	Edla	TW	23.54	72.06	288.7	-2.10	-24.8	-8.0
312	Diyodar	TW	24.10	71.74	207.3	-3.60	-24.2	4.6
313	Diyodar	TW	24.10	71.74	207.3	-3.58	-25.3	3.4
314	Tharad	TW	24.41	71.64	201.2	-0.89	-24.9	-17.8
316	Agathala	TW	24.29	71.88	137.2	0.50	-33.3	-37.3
317	Sujanipur	TW	23.89	72.11	91.4	-1.72	-24.1	-10.3
318	Sujanipur	TW	23.90	72.12	326.1	-3.28	-23.9	2.3
319	Sujanipur	TW	23.91	72.12	39.6	-3.63	-29.2	-0.2
320	Kuwarva	TW	24.04	71.90	186.6	4.46	-28.2	-63.9
321	Kharia	TW	23.94	71.83	158.5	-3.28	-32.5	-6.3
322	Sami	TW	23.70	71.78	298.7	-3.34	-24.0	2.8
323	Hedva	TW	23.57	72.34	82.3	-3.14	-21.6	3.5
324	Kuder	TW	23.70	71.87	262.1	0.25	-23.1	-25.1
325	Patan	TW	23.84	72.11	198.1	-3.11	-23.0	1.9
326	Patan	TW	23.84	72.11	129.5	-2.90	-22.1	1.1
327	Patan	TW	23.84	72.11	60.0	-1.45	-23.5	-11.9
328	Jitoda	TW	23.74	72.15	312.7	-2.48	-20.5	-0.6
329	Jitoda	TW	23.74	72.15	448.1	-2.79	-13.6	8.8
330	Kamboi	TW	23.67	72.02	213.4	-2.97	-15.6	8.1
331	Muthia	TW	23.09	72.69	141.7	-3.08	-20.6	4.1
332	Paliya	TW	23.18	72.83	118.9	-2.82	-21.5	1.0
333	Punsari	TW	23.39	73.10	32.3	-3.58	-25.5	3.1
334	Dalani Muwadi	TW	23.36	72.88	91.4	-3.47	-24.6	3.1
335	Rojad	HP	23.35	73.09	28.7	-0.70	-22.1	-16.5
336	Vadrad	TW	23.42	72.89	57.9	-2.98	-25.2	-1.4
337	Tejpur	TW	23.39	72.81	160.0	0.12	-23.2	-24.2
338	Navalpur	TW	23.60	72.90	121.9	-2.81	-21.8	0.7
339	Dhanap	TW	23.26	72.75	167.6	-3.11	-23.3	1.5
340	Indroda Park	TW	23.19	72.65	106.7	-1.79	-23.0	-8.7
341	Rupawati	TW	23.00	72.30	213.4	3.21	-24.4	-50.1
342	Sokali	TW	23.10	72.11	93.0	-2.60	-24.2	-3.4
343	Dulapur	TW	23.02	71.58	61.0	-3.13	-23.0	2.0
355	Salajada	TW	22.80	72.39		-3.32	-23.2	3.4
356	Salajada	TW	22.79	72.39	198.4	-3.27	-22.9	3.3
357	Salajada	TW	22.79	72.39	93.0	-2.89	-19.9	3.2
358	Gundi	TA	22.55	72.23	289.6	-3.56	-25.2	3.3
359	Shiyal	TW	22.68	72.16	274.3	-3.45	-26.1	1.5
360	Padgol	TW	22.59	72.84	137.2	-3.07	-21.5	3.0

Table 4.4 continues

CBGW Sample No.	Location name	Well type	Lat. (°N)	Long. (°E)	Depth bgl (m)	$\delta^{18}\text{O}$ (‰)	δD (‰)	d -excess (‰)
361	Morad	TW	22.54	72.86	91.4	-2.76	-21.2	0.8
362	Gumadia	TW	22.76	73.23	48.8	-2.62	-21.0	-0.1
363	Tuwa	TS	22.80	73.46	1	-1.94	-14.8	0.7
364	Tuwa	TS	22.80	73.46	1	-1.34	-14.4	-3.7
365	Tuwa	TS	22.80	73.46	1	-1.45	-14.6	-3.0
366	Tuwa	TS	22.80	73.46	1	-0.86	-12.5	-5.6
367	Dholera	TA	22.25	72.19	168	-3.71	-27.4	2.3
Average of all groundwater samples						-1.2±1.3	-22± 5	-4.5 ± 11

Table 4.5 Details of rainwater sampling sites together with values of $\delta^{18}\text{O}$, δD and d -excess in the NGC region. (Da = Dantiwada; Dh = Dharoi; Un = Unjha).

Sample No.	Rain fall (mm)	$\delta^{18}\text{O}$ (‰)	δD (‰)	d -excess (‰)
Da-1	32.2	-4.04	-32.9	-0.6
Da-2	61.9	-0.45	-1.7	1.9
Da-3	4.5	-0.24	-1.1	0.8
Da-4	4.4	1.75	9.3	-4.7
Da-5	31.2	-4.02	-39.9	-7.7
Da-6	33.2	-9.49	-81.5	-5.6
Da-8	126.6	-3.59	-26.3	2.4
Da-9	11.1	0.06	3.0	2.5
Da-10	96.4	-3.92	-31.4	0.0
Da-11	6	0.97	2.2	-5.6
Da-14	15.1	-2.66	-54.8	-33.5
Da-15	203.1	-7.05	-46.9	9.5
Da-17	100.5	-4.02	-29.4	2.7
Dh-1	70.8	-2.72	-20.9	0.9
Dh-2	42.2	-1.10	-3.6	5.3
Dh-3	38.2	-0.81	-5.7	0.7
Dh-4	28.8	0.81	4.8	-1.7
Dh-5	18.4	1.08	7.5	-1.1
Dh-6	28.6	-6.04	-46.1	2.2
Dh-18	145	-7.36	-57.7	1.2
Dh-19	620	-4.10	-32.4	0.4
Dh-20	56	-5.36	-46.5	-3.6
Amount weighted average		-4.3 ± 2.1	-33 ± 16	1.2 ± 4.8
Un-1	---	-3.51	-23.7	4.4
Un-2	---	-2.08	-17.5	-0.8
Un-3	---	1.08	-5.6	-14.3

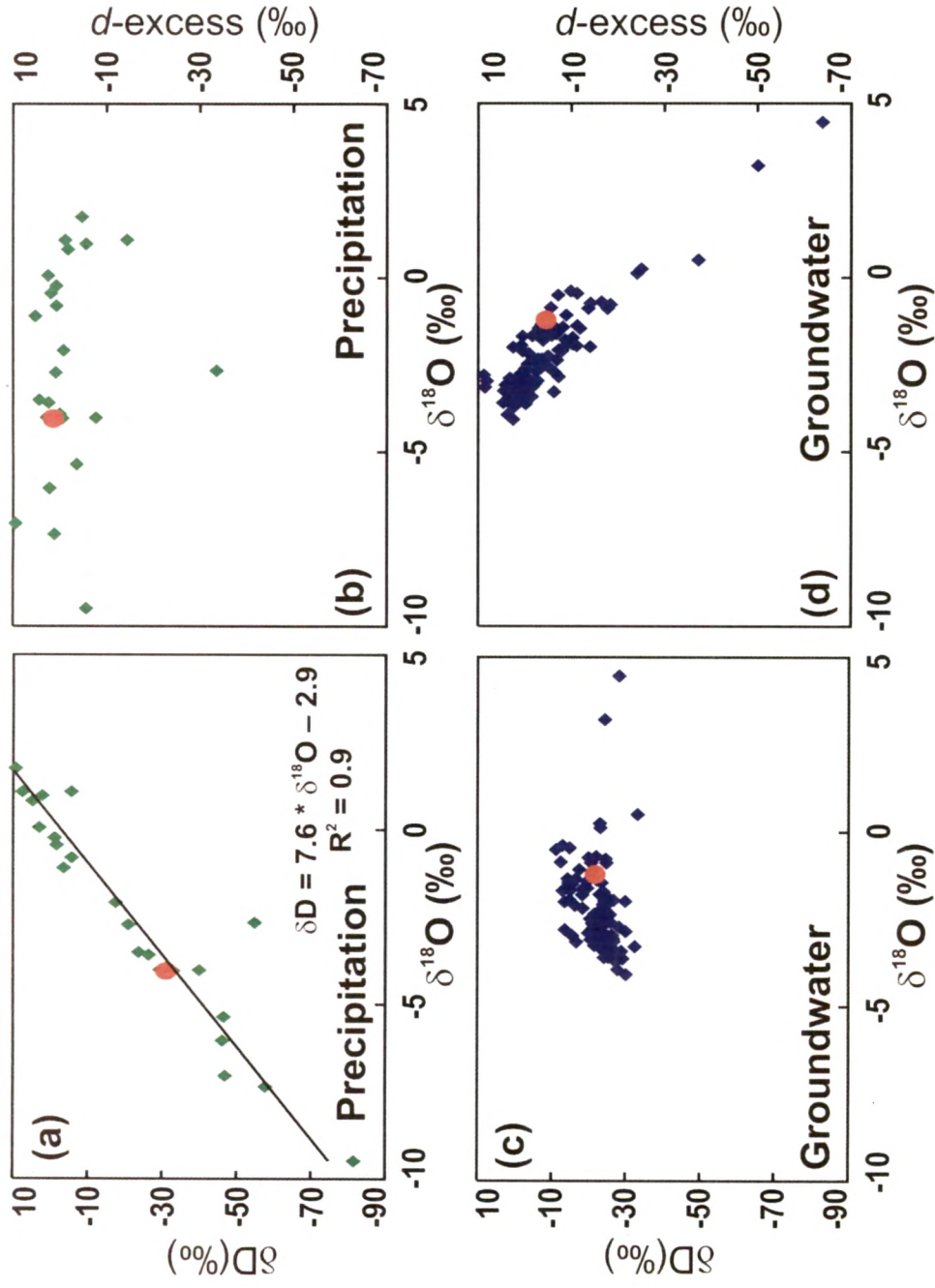


Figure 4.15 $\delta^{18}O$ vs. δD and $\delta^{18}O$ vs. d -excess for precipitation (a and b) and for groundwater samples (c and d). The average values for respective parameters in each figure are shown by big circle. In case of precipitation, the average value is amount weighted.

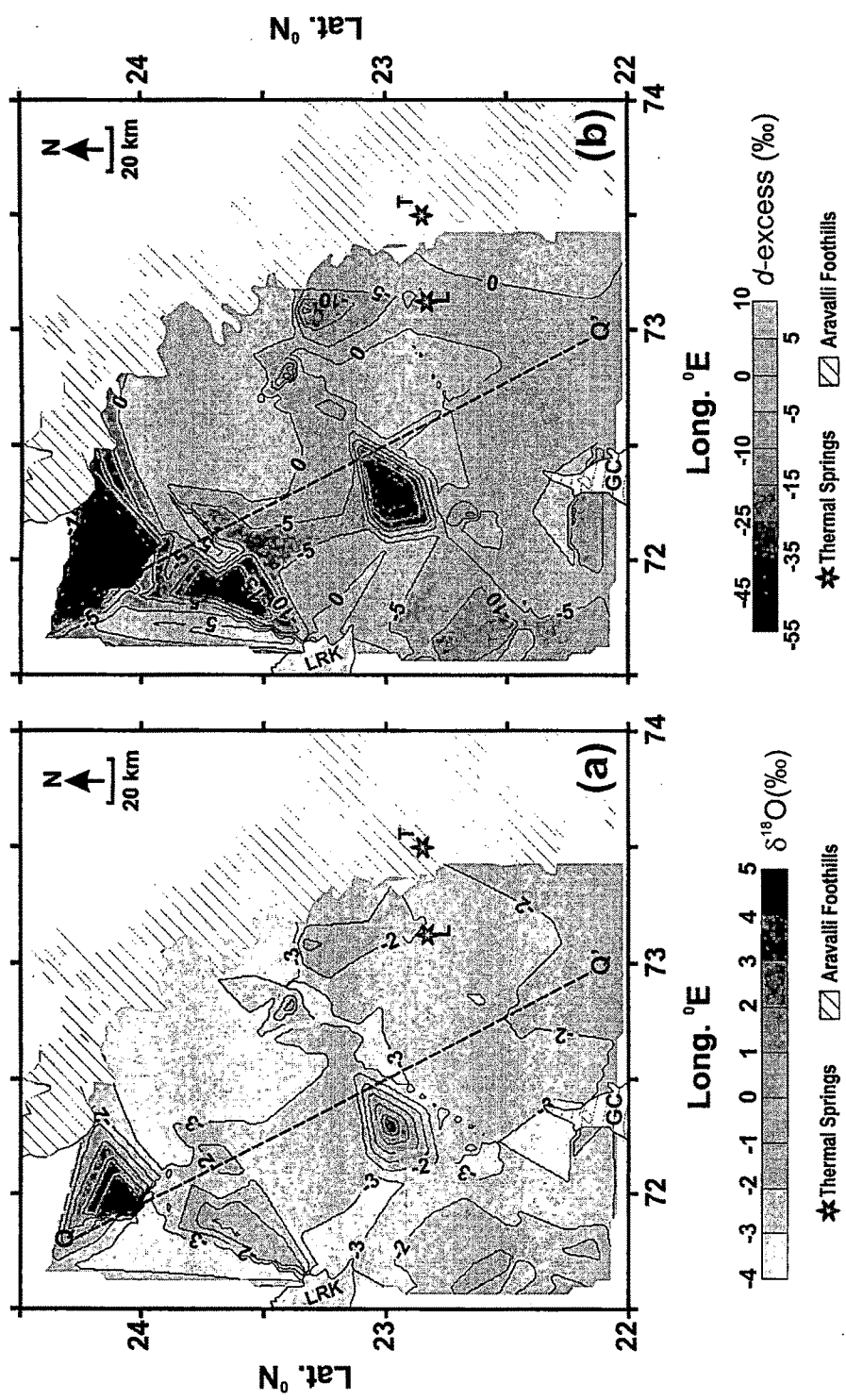


Figure 4.16 Isoline map of (a) $\delta^{18}\text{O}$ and (b) d -excess of groundwater from NGC region. Line QQ' representing the central linear belt of high fluoride (in Figure 4.5) and high EC (in Figure 4.8) is superposed for comparison.

The $\delta^{18}\text{O}$ and δD values of the fortnightly precipitation samples are linearly correlated (Figure 4.15a) and the regression line (LMWL) has a slope of (7.6 ± 0.6) with an intercept of $(-2.9 \pm 2.2\text{‰})$. The amount weighted average values of $\delta^{18}\text{O}$ and δD for precipitation samples are $-4.3 \pm 2.1\text{‰}$ and $-33 \pm 16\text{‰}$ respectively. Using $\delta^{18}\text{O}$ and δD values of each sample, d-excess values are calculated ($= \delta\text{D} - 8 \cdot \delta^{18}\text{O}$) and plotted against $\delta^{18}\text{O}$ in Figure 4.15b. The d-excess values of the precipitation samples lie between -10‰ and $+10\text{‰}$, except for two samples having d-excess value of -14‰ and -33‰ . The amount weighted average d-excess value for precipitation samples is $1.2 \pm 4.8\text{‰}$.

A plot (Figure 4.15c) of $\delta^{18}\text{O}$ vs. δD for groundwater shows a cluster of data points and does not warrant further statistically meaningful analyses. Isotopic ratios of the groundwater samples have a narrow range of variation with average value of $-1.2 \pm 1.3\text{‰}$ for $\delta^{18}\text{O}$ and $-22 \pm 5\text{‰}$ for δD .

A plot of $\delta^{18}\text{O}$ vs. d-excess for groundwater samples (Figure 4.15d) shows a decrease in d-excess values with increase in $\delta^{18}\text{O}$. Unlike precipitation samples, several groundwater samples have d-excess values lower than -10‰ . The average d-excess value of groundwater samples is $-4.5 \pm 11\text{‰}$.

The geographical distributions of $\delta^{18}\text{O}$ and d-excess of groundwater in the NGC region are shown in Figure 4.16. It is seen from Figure 4.16a that in most part of the study area $\delta^{18}\text{O}$ values are $< -3\text{‰}$. There is, however, a prominent geographical belt with relatively higher $\delta^{18}\text{O}$ values ($> -3\text{‰}$). Several small regions with even higher values of $\delta^{18}\text{O}$ ($> -2\text{‰}$) are located within this belt. It is seen from Figure 4.16b that d-excess values of ground waters in large part of the NGC region are between 0 to 5‰ . However, a prominent geographical belt with relatively lower d-excess ($< 0\text{‰}$) is also seen. Several small regions with much lower d-excess values ($< -15\text{‰}$) are located within this broad belt. Line QQ' which marks the region of high fluoride (Figure 4.5) and high EC (Figure 4.8), is also superposed on Figure 4.16.

4.1.6 Groundwater Dating

Three different methods, namely ^{14}C , ^4He and $^4\text{He}/^{222}\text{Rn}$, were employed for estimating the age of ground waters in the study area. The estimated groundwater ages by each of these methods are described in the following.

Table 4.6 Details of the groundwater sampling sites together with measured values of $\delta^{13}\text{C}$, pmC, ^{14}C ages corrected for A_0 as well as un-corrected for A_0 . (pmC = percentage modern carbon; TDIC = total dissolved inorganic carbon; bdl = below detection limit; A_0 = initial activity; CBGW = Cambay Basin Ground Water)

CBGW No.	Location name	Lat. (°N)	Long. (°E)	$\delta^{13}\text{C}_{\text{TDIC}}$ (‰)	pmc	^{14}C ages (kaBP) [A_0 Uncorrected]	^{14}C ages (kaBP) [A_0 corrected]
208	Maniyor	23.82	72.96	-10.78	115±1.1	modern	modern
209	Dharewada	23.98	72.39	-8.99	58±0.7	4.45±0.09	1.5±0.14
210	Ganguva	24.16	72.73	-10.4	100±0.9	modern	modern
211	Chadotar	24.21	72.4	-8.62	99±0.9	modern	modern
212	Bhadath	24.34	72.2	-8.26	102±1.0	modern	modern
215	Tharad	24.41	71.64	-8.47	2.3±0.2	31.21±0.68	27.6±0.73
216	Jitoda	23.74	72.15	-7.26	35±0.5	8.63±0.12	3.9±0.16
218	Sami	23.7	71.78	-11.74	0.61±0.2	42.2±2.6	41.3±2.73
219	Wavadi	23.92	72.52	-9.56	90±1.0	0.92±0.09	modern
220	Pilwai	23.53	72.69	-11.56	22±0.4	12.53±0.14	11.5±0.17
222	Heduva	23.57	72.34	-9.17	37±0.5	8.19±0.1	5.3±0.14
223	Vaghpur	23.68	73.42	-11.34	81±0.8	1.73±0.08	0.6±0.11
224	Edla	23.54	72.06	-10.12	1.7±0.2	33.75±0.88	31.6±0.98
225	Sherisa	23.2	72.48	-9.47	50±0.6	5.75±0.1	3.1±0.13
320	Kuwarava	24.04	71.9	-8.81	2.8±0.3	29.64±0.97	26.3±0.90
331	Muthia	23.09	72.69	-8.6	68±0.8	3.15±0.1	modern
333	Punsari	23.39	73.1	-9.11	89±0.8	1.01±0.07	modern
336	Vadrad	23.42	72.89	-9.28	99±0.9	modern	modern
337	Tajpur	23.39	72.81	-11.6	68±0.7	3.25±0.08	2.2±0.11
341	Rupawati	23	72.3	-9.29	1.8±0.2	33.29±0.89	30.4±0.93
344	Gajanav	22.92	71.36	-9.75	80±0.7	1.82±0.08	modern
351	Navagam	22.62	71.18	-11.11	93±0.8	0.61±0.08	modern
355	Salajada	22.8	72.39	-8.23	9.5±0.2	19.5±0.21	15.7±0.20
358	Gundi	22.55	72.23	-21.36	b.d.l.	>45	>45
360	Padgol	22.59	72.84	-9.7	49±0.5	5.87±0.09	3.5±0.12
362	Gumadia	22.76	73.23	-8.94	84±0.8	1.47±0.08	modern
RC-1	PRL	23.04	72.54	-13	40±0.6	7.58±0.12	7.6±0.14

Initial activity A_0 (Un-corrected) = 100 % Modern;

$$\text{Initial activity } A_0 \text{ (corrected)} = \frac{\delta^{13}\text{C}_{\text{TDIC}}}{\delta^{13}\text{C}_{\text{soil}} - \epsilon} 100;$$

$$\delta^{13}\text{C}_{\text{soil}} = -22\text{‰}; \epsilon = -9\text{‰}.$$

4.1.6.1 ^{14}C Dating

Details of the (i) sampled tubewell locations; and values of (ii) percentage modern carbon (pmC); (iii) $\delta^{13}\text{C}_{\text{TDIC}}$; (iv) ^{14}C ages un-corrected for initial activity (A_0) as well as (v) ^{14}C ages corrected for A_0 , are given in Table 4.6. The isoline map of radiocarbon ages is shown in Figure 4.17. It is seen that the groundwater ^{14}C ages progressively increase from <2 kaBP in the recharge area (foothills of Aravalli mountains) to a limiting value of >35 kaBP in the LRK-NS-GC tract. Within the Cambay Basin, ^{14}C age isolines are nearly parallel to each other and the horizontal distance between successive 5 kaBP isolines is nearly constant.

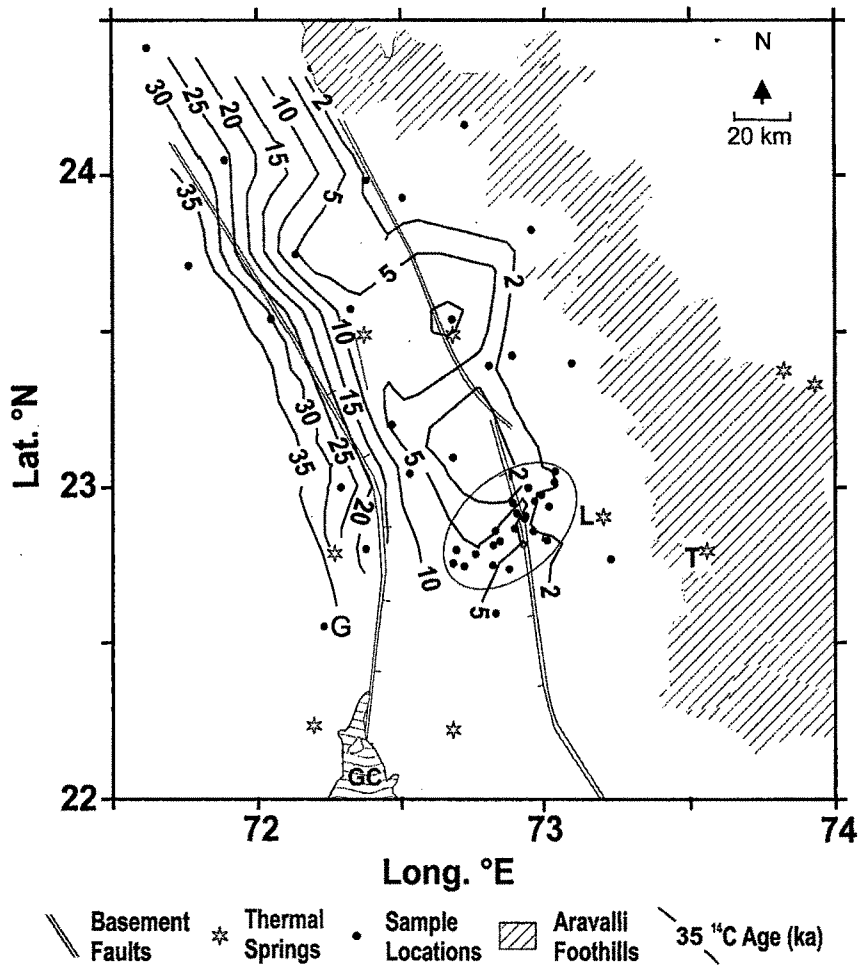


Figure 4.17 Isoline map of groundwater Radiocarbon ages, along with sampling locations. Sampling locations of an earlier study (Borole et al, 1979) are enclosed in an ellipse. Within the Cambay basin the groundwater ^{14}C ages increase progressively towards the WCBBF, beyond which a limiting ^{14}C age of >35 kaBP is observed. Dots indicate sampling locations. L, T and G respectively indicate the locations of thermal springs at Lasundra, Tuwa and a free flowing thermal artesian well at Gundi. The groundwater age gradient along BB' is shown in Figure 4.21.

4.1.6.2 ^4He Dating

The details of the (i) sampled well locations; and (ii) values of estimated ^4He ages for helium release factor (Λ_{He}) of 1 and 0.4 are given in Table 4.1. The isoline map of estimated ^4He ages of the groundwater in the NGC region is shown in Figure 4.18. The ^4He ages are calculated (see section 2.6.2) based on the measured concentration of Uranium ($U = 1.07 \text{ ppm}$) and Thorium ($Th = 7.54 \text{ ppm}$), and assuming the value of density ($\rho = 2.6 \text{ g cm}^{-3}$, porosity ($n = 20\%$) and helium release factor ($\Lambda_{\text{He}} = 1$). With these values, the 5 ppmAEU He_{ex} (see Figure 4.1) corresponds to groundwater ^4He age of $\sim 15 \text{ kaBP}$ (Figure 4.18). If, however, the value of Λ_{He} is assumed to be 0.4, the 5 ppmAEU He_{ex} would correspond to ^4He age of $\sim 37 \text{ kaBP}$ and would be in close agreement with the groundwater ^{14}C age isoline of $>35 \text{ kaBP}$ (Figure 4.17).

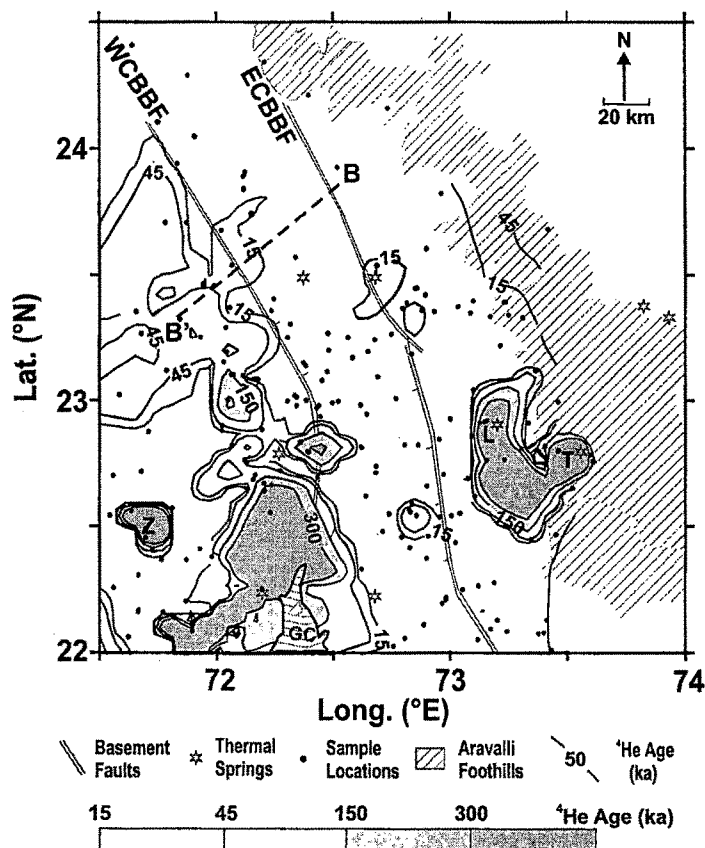


Figure 4.18 Isoline map of estimated ^4He ages of groundwater from the NGC region (for helium release factor; $\Lambda_{\text{He}} = 1$). Isoline of 15 kaBP runs almost along the WCBBF. This isoline will correspond to the ^4He age of $\sim 37 \text{ kaBP}$ for $\Lambda_{\text{He}} = 0.4$ (See Section 2.6.2). Dots indicate sampling locations. L, T and Z respectively indicate the locations of thermal springs at Lasundra, Tuwa, and the tubewell in Zinzawadar. The groundwater age gradient along BB' is shown in Figure 4.21.

Table 4.7 Results of $^4\text{He}/^{222}\text{Rn}$ groundwater dating. Calculations are based on: $\text{Th}/\text{U} = 7.1 \pm 4.3$; $\Lambda_{\text{Rn}}/\Lambda_{\text{He}} = 0.4$; $\rho = 2.6 \text{ g cm}^{-3}$; $n = 20\%$.

CBGW Sample No.	Location Name	Lat. (°N)	Long. (°E)	^{222}Rn activity (dpm/l)	He_{ex} (ppmAEU)	$^4\text{He}/^{222}\text{Rn}$ ages (kaBP)
312	Diyodar	24.10	71.74	945±83	1.9	16
313	Diyodar	24.10	71.74	987±91	1.2	10
314	Tharad	24.41	71.64	810±65	33.7	330
316	Agathala	24.29	71.88	742±67	0.6	6
317	Sujnipur	23.89	72.11	1077±87	0.0	0
318	Sujnipur	23.90	72.12	1551±124	5.5	28
319	Sujnipur	23.90	72.12	629±57	0.0	0
320	Kuwarva	24.04	71.90	599±57	0.0	0
321	Kharia	23.94	71.83	916±83	0.0	0
322	Sami	23.70	71.78	137±30	44.1	2553
323	Hedwa	23.57	72.34	469±48	1.2	20
324	Kuder	23.73	72.19	462±58	1.2	20
325	Patan	23.84	72.11	822±72	0.0	0
326	Patan	23.84	72.11	673±63	0.3	3
327	Patan	23.84	72.11	261±36	0.0	0
328	Jitoda	23.74	72.15	1114±106	0.6	4
329	Jitoda	23.74	72.15	1871±144	9.9	42
330	Kamboi	23.67	72.02	1253±97	6.4	41
331	Muthia	23.09	72.69	481±24	0.0	0
332	Paliya	23.18	72.83	1262±52	0.0	0
333	Punsari	23.39	73.10	522±26	0.0	0
334	Dalani Muwadi	23.36	72.88	279±19	13.3	378
335	Rojad	23.35	73.09	281±19	0.0	0
336	Vadrad	23.42	72.89	923±41	1.7	15
337	Tajpur	23.39	72.81	721±36	0.0	0
338	Navalpur	23.60	72.90	245±17	0.0	0
339	Dhanap	23.26	72.75	643±34	0.0	0
340	Indroda Park	23.19	72.65	231±19	0.0	0
341	Rupawati	22.99	72.30	908±41	3.5	30
342	Sokali	23.10	72.11	657±31	0.7	8
343	Dudapur	23.02	71.58	2595±110	44.5	136
355	Salajada	22.80	72.39	480±28	0.9	15
356	Salajada	22.79	72.39	379±25	0.9	18

Table 4.7 continues

CBGW Sample No.	Location Name	Lat. (°N)	Long. (°E)	^{222}Rn activity (dpm/l)	He_{ex} (ppmAEU)	$^4\text{He}/^{222}\text{Rn}$ ages (kaBP)
357	Salajada	22.79	72.39	426±30	0.3	5
358	Gundi	22.55	72.23	301±18	175.3	4624
359	Shiyal	22.68	72.16	262±17	230.1	6958
360	Padgol	22.59	72.84	468±24	1.3	23
361	Morad	22.54	72.86	322±19	0.0	0
362	Gumadia	22.76	73.23	442±22	0.0	0
363	Tuwa	22.80	73.46	62571±2405	405.0	51
364	Tuwa	22.80	73.46	32538±1272	277.0	68
366	Tuwa	22.80	73.46	36394±1413	253.0	55
367	Dholera	22.25	72.19	362±17	465.0	10189

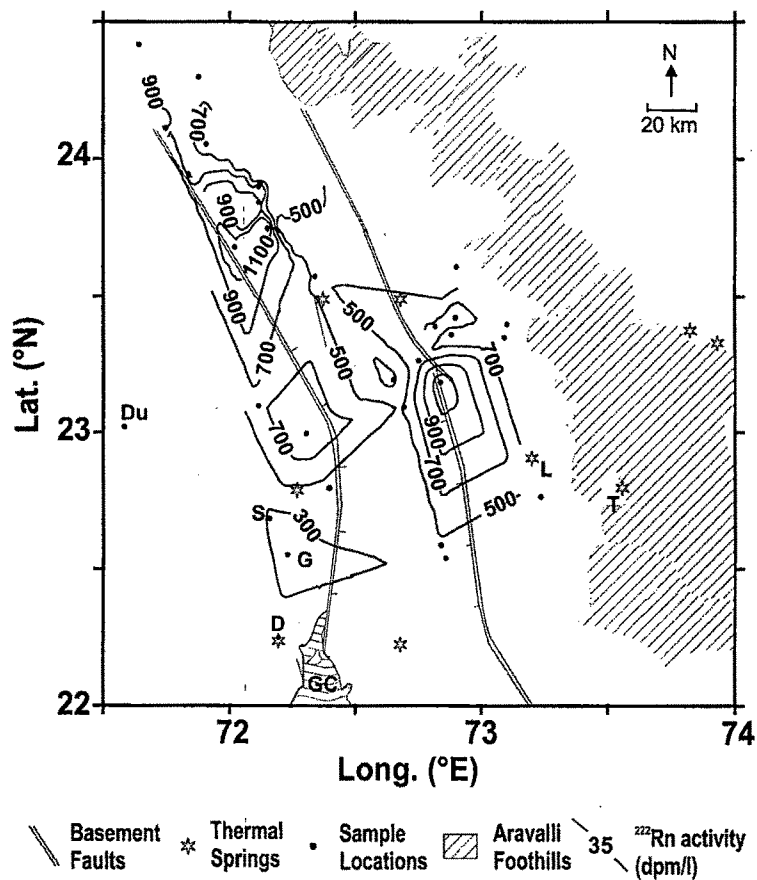


Figure 4.19 Iso-line map of groundwater $^4\text{He}/^{222}\text{Rn}$ ages in the NGC region for $\text{Th}/\text{U} = 7.1$; $\Lambda_{\text{Rn}}/\Lambda_{\text{He}} = 0.4$; $\rho = 2.6 \text{ g cm}^{-3}$ and $n = 20\%$. Samples with $>10\text{ppmAEU}$ 'excess He' and/or $>2000 \text{ dpm/l}$ ^{222}Rn were excluded during contouring. Dots indicate sampling locations. The groundwater age gradient along BB' is shown in Figure 4.21.

4.1.6.3 $^4\text{He}/^{222}\text{Rn}$ Dating

Details of the (i) sampled well locations; and values of (ii) ^{222}Rn activity; (iii) He_{ex} ; and (iv) estimated $^{222}\text{Rn}/^4\text{He}$ ages are given in Table 4.7. The isoline map of estimated $^4\text{He}/^{222}\text{Rn}$ ages of the groundwater in the NGC region is shown in Figure 4.19. The $^4\text{He}/^{222}\text{Rn}$ ages are calculated (see Section 2.6.3) based on Th/U concentration ratio = 7.1; $\rho = 2.6 \text{ g cm}^{-3}$; $n = 20\%$; and release factor ratio ($\Lambda_{\text{Rn}}/\Lambda_{\text{He}}$) of 0.4. A gradual WSW progression of $^4\text{He}/^{222}\text{Rn}$ ages, away from the recharge area, is seen in Figure 4.19 similar to ^{14}C age progression (Figure 4.17). The $^4\text{He}/^{222}\text{Rn}$ ages were obtained using release factor ratio ($\Lambda_{\text{Rn}}/\Lambda_{\text{He}}$) of 0.4 which provided the best match with the ^{14}C age gradient.

4.2 Discussion

The salient points of the results from various geochemical and isotopic investigations are discussed in the following to understand respective roles of geohydrological, tectonic, topographic and palaeoclimatic factors in governing the observed geochemical and isotopic properties of groundwater in NGC region.

4.2.1 Groundwater Helium and Temperature

It is seen from Figure 4.1 and Figure 4.2 that areas of high He_{ex} (>15 ppm AEU) in groundwater are generally associated with areas of high groundwater temperatures (>35°C). Such areas are found to (i) lie along the major basement faults (ECBBF and WCBBF); (ii) overlie sympathetic faults both parallel and orthogonal to major faults; and (iii) overlie regions of thermal springs. Despite this geographical correlation between high He_{ex} and high temperature of groundwater, no quantitative correlation was seen between the two (Figure 4.3). This dichotomy is even more pronounced when comparing two samples – one with highest He_{ex} (CBGW-120; Figure 4.1; Table 4.1; 2843 ppmAEU; 34°C) from Zinzawadar and the other with highest groundwater temperature (CBGW-18; Table 4.1; Figure 4.1; 137 ppmAEU; 61°C).

It is also seen from Figure 4.18 that estimated ^4He ages of groundwater right in the recharge area, particularly around thermal springs of Tuwa and Lasundra, are >100 kaBP. This implies that these ground waters have been accumulating helium from *in-situ* sources alone (i.e. from aquifer/ rock volume that groundwater comes in contact with) for more than 100 kaBP. Such a long residence time, particularly in the recharge area is not compatible with the hydrogeology and the ^{14}C age (<2 kaBP; Figure 4.17) of groundwater in this region. Alternatively, local uranium mineralization can also cause high He_{ex} . However, unusually high ^{222}Rn activity is not observed (except for thermal springs at Tuwa; Table 4.7) in the region. No other evidence of near surface uranium

mineralization has been reported from this region discounting the possibility of near surface uranium mineralization as a source for the observed He_{ex} in groundwater.

In case of groundwater far away from the recharge area, for example, at Zinzawadar (Figure 4.18), the required *in-situ* accumulation time for the observed He_{ex} (2843 ppmAEU), would be >8,000 kaBP. Groundwater inliers with such a high residence time surrounded by younger ground waters are hydro-geologically untenable even though the ^{14}C ages (Figure 4.17) of groundwater in this region are beyond the limiting age of >35 kaBP and the ^4He ages (Figure 4.18) are >45 kaBP little eastward of Zinzawadar. However, it is possible that observed high He_{ex} in certain groundwater inliers are due to injection from a deeper source that derives helium from much larger aquifer/ rock volume. This is also suggested by the geographical coincidence of areas with groundwater He_{ex} and high temperature and their position over the basement faults. In this scheme, deep subsurface faults provide routes for upward migration of deeper fluids having both very high concentration of helium and high temperature. Lack of any quantitative relationship between He_{ex} and groundwater temperature, however, indicates the possibility that many localized sources with their varying helium concentration and fluid temperature may be involved in transferring helium and/ or heat from deeper levels to shallower aquifers. This conceptual frame work is explained further in the following.

In the presence of concentration gradient, gaseous ^4He can physically diffuse out of rocks/minerals through the network of 100-200Å wide nano-pores present in the rock or grain body (Rama and Moore, 1984). If network of such diffusive pathways opens out into a bigger fault or fracture, gaseous helium can diffuse out through such preferential pathways and dissolve in the deep ground waters, considerably increasing its dissolved helium content. Plumes of such deep fluids can be injected (under hydrostatic pressure due to geothermal heat) into relatively shallow aquifers through underlying basement faults and fractures. This can result in localized pockets of very high He_{ex} and temperature in groundwater in such a way that these will be aligned around the basement fractures/ faults. It is, thus, possible for the groundwater overlying a fractured zone, to acquire the helium produced elsewhere (within or below the basement). There may be several such plumes in a large fractured terrain. The amount of helium and heat transferred to shallower layers would then depend on the concentration of helium and temperature of the fluid in a particular plume. If a single well-mixed fluid source was contributing helium and heat to shallower groundwater throughout the region, one could expect a relationship between observed helium concentration and the groundwater temperature. Absence of any such correlation is, therefore, a clear indication that several

localized fluid injections are involved and deep fractures and faults provide pathways for upward migration of deeper fluids.

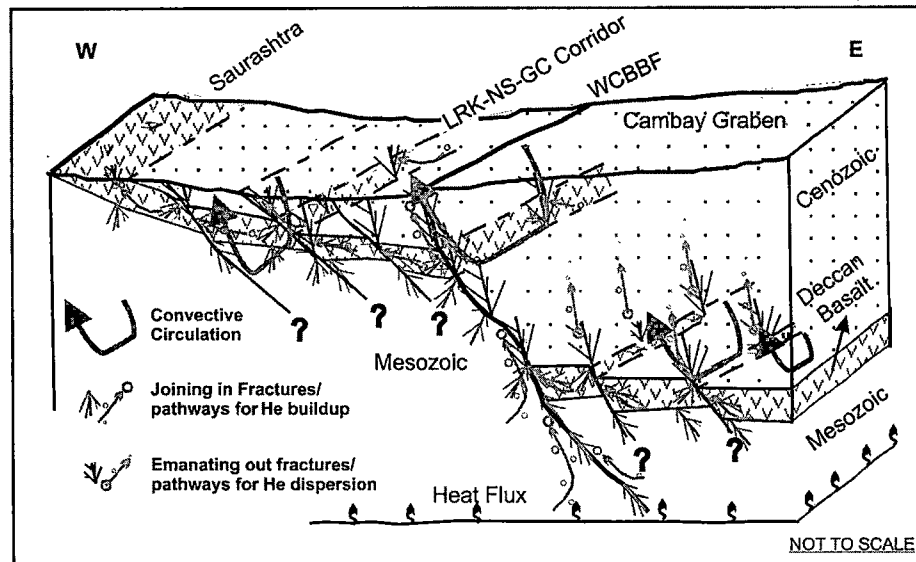


Figure 4.20 A conceptual tectono-hydrothermal model to explain the origin and observed geographical distribution of He_{ex} and high temperature of groundwater in NGC region. The set of braided fractures joining the major fault traces is indicative of migration of helium from micro-cracks into macro-fractures, eventually joining the conduits provided by the major fractures and faults. The joining-in fractures (indicated by an arrow with a circle at top) thus acts as the pathway for build-up of helium in deep groundwater. Another set of braided fractures emanating out of the major fault traces is indicative of pathway that the upward migrating helium follows through the overlying sedimentary cover leading to dispersion/diffusion. In both cases, the size of circles schematically depicts the changing helium concentration during upward migration of deeper fluids. The arrows leading to major faults depict the preferred pathways for migration of radiogenic helium derived from a large area. The thick arrows indicate the hydrothermal circulation along major faults, facilitated by high heat flux.

The above scheme can be presented in the form of a conceptual tectono-hydrothermal model for the NGC region depicted in Figure 4.20. The radiogenic helium produced in large volume of rocks within or below the basement migrates through micro-cracks into braided and interconnected fractures and dissolves in deep fluids/groundwater. Such deep fluids could even be of lower crust/ upper mantle origin but could also arise from downward migration of meteoric water from other locations through the pathways provided by deep fractures and fissures. This could result in setting up of a hydrothermal circulation along the deep seated fractures and fissures. The extent to which these deep fluids may have high concentration of helium is governed by interconnection of micro-cracks and fractures and the temperature is governed by the

depth up to which a particular hydrothermal circulation cell penetrates. These factors will depend on the local geology affecting individual hydrothermal cells and, therefore, have local variation. The braided fractures emanating out from the major faults can also facilitate upward migration of helium through the overlying sedimentary cover. Sedimentary formations are characterized by uniform and high density pores that cause almost omni-directional migration of helium while crystalline formations have relatively small density of interconnected fractures and fissures governing the migration of helium. As a result, sedimentary formations cause large dispersion of the upward migratory helium plume whereas the crystalline formations tend to act as local source of helium plumes.

In addition to mixing of deep fluids with local groundwater and their dispersion in sedimentary formation, the helium can diffuse omni-directionally within the aquifer, be transported along with groundwater or diffuse out into atmosphere through the water-air interface. Similarly, heat is dissipated both through conduction and convection (along with groundwater flow). This is the reason why both helium and temperature anomalies are considerably subdued over the Cambay basin (between the ECBBF and the WCBBF) with ~3km thick sedimentary cover.

4.2.2 Fluoride and Electrical Conductivity

As seen from Figure 4.6, within the Cambay Basin certain sub-aquifer depth zones have high concentration (>1.5 ppm) of groundwater fluoride. As already mentioned, in view of the general topographic gradient, a particular depth (bgl) traces approximately the same sub-aquifer (see Figure 1.6) in different parts of the region. Based on the above arguments and investigation of 5 tubewells tapping various depth zones within a small region, it was further contended that if a particular tubewell taps the identified high fluoride depth zone (Table 4.3); its groundwater shows high concentration of fluoride (Figure 4.7). However, it was also mentioned that the above hypothesis could not be confirmed for the entire NGC regional aquifer system due to limited availability of tubewells providing suitable conditions (such as at Chadotar and Kuwarva). Further, it is also noticed that the entire NGC regional aquifer system comprises Quaternary sediments derived from fluvial transport of weathered, largely granitic, rocks from the Aravalli Mountains. Therefore, the bulk mineral assemblage of different sub-aquifer depth zones, though not expected to be significantly different from each other, may have some pockets at certain depths with accumulation of fluoride bearing minerals. But to expect such pockets forming regionally extensive sub-aquifer zones, contributing high fluoride to groundwater may be quite speculative.

Instead, the fluoride distribution in the NGC region is explained on the basis of a hydrological model comprising a recharge area in the Aravalli foothills, grading into the confined aquifer (Figure 1.6) towards LRK-NS-GC belt. The groundwater in this system moves through the confined aquifer with the dissolved chemical characteristics acquired from the recharge area but aging progressively as it moves away from the recharge area. In this model interaction with aquifer matrix after the zone of effective confinement is not considered to significantly alter the chemical properties of groundwater.

Geographical distribution of dissolved fluoride in groundwater of NGC region revealed that areas of high fluoride concentrations (>1.5 ppm) are aligned around four lines PP', QQ', RR' and SS' (Figure 4.5). Of these, three lines (PP', QQ' and RR') are trending NW-SE and are roughly parallel to the Aravalli foothills. These linear belts of high groundwater fluoride are distinctly separated by areas with relatively lower fluoride content. The fourth linear belt (SS') is trending nearly E-W and connects the regions of thermal springs of Tuwa and Lasundra to the low lying area around Nalsarovar. The groundwater pockets with high fluoride along these linear belts also geographically coincide with groundwater pockets of high salinity (EC >2 mS; Figure 4.8), excepting some pockets in the recharge area in the Aravalli foothills.

The mineral assemblage of the granites in the Aravalli foothills includes fluoride-rich minerals such as fluorite, apatite, biotite and amphiboles among several others. These granites are invaded by dykes of pegmatite that also contain xenoliths of amphibolites which are known for their high fluoride content. Since the sediments of the NGC region have been derived from the weathering of the Aravalli Mountains, it is possible that the aquifer matrix contains some fluoride rich minerals. Based on the fact that dissolved salt content of groundwater is to some extent related to leaching from the aquifer matrix, the high fluoride concentration in ground waters of NGC region was hitherto believed to be related to its residence time in the aquifer (Patel, 1986). However, comparison of isolines of fluoride (Figure 4.5) and isolines of ^{14}C ages (Figure 4.17) revealed that this may not be true.

The groundwater ^{14}C ages (Figure 4.17) progressively increase from <2 kaBP in the recharge area (Aravalli foothills) to >35 kaBP in the low lying belt linking LRK-NS-GC. If the residence time of groundwater indeed controlled its fluoride content, it should have progressively increased with the ^{14}C ages, as a function of distance from the recharge area. This, however, is not supported by Figure 4.5, which shows that three almost parallel linear geographical belts of high groundwater fluoride are clearly separated by areas with relatively lower fluoride content. The alternating high and low fluoride concentration in groundwater from confined aquifers suggest the possibility of an

additional (other than progressive leaching from mineral grains) non-geological control on the fluoride concentration in groundwater of NGC region.

The enhanced aridity is generally associated with (i) increased evaporation; (ii) decreased rainfall; and (iii) increased dry deposition. Some imprints of evaporation and dry deposition in the present climate are seen in the ion concentration (Section 4.1.4) and stable isotope composition (Section 4.1.5) of modern rainfall. The significant control of dry deposition is seen in the variation of fluoride and EC of fortnightly accumulated rain water samples (Figure 4.11). It is seen that variation of fluoride and EC in rainwater are not related to the amount of rainfall. Therefore, the increased dry deposition seems to be the source of increased fluoride concentration and EC in certain fortnightly accumulated rainwater samples. It is also seen that variations in fluoride concentration and EC of rainwater are nearly proportional to each other (Figure 4.13). Therefore, the surface water, infiltrating to form the shallow groundwater can have both higher concentration of fluoride and higher EC due to enhanced dry deposition and higher evaporation during periods of increased aridity compared to preceding or succeeding periods of relatively wetter climate.

It is seen (Figure 4.5 and Figure 4.17) that the confined groundwater in the central high fluoride groundwater belt (QQ') within the Cambay Basin corresponds to groundwater ^{14}C age in the range 15-25 kaBP. The period around 20 kaBP, corresponding to the Last Glacial Maxima (LGM), is known to be a period of enhanced aridity in the NGC region (Prasad and Gupta, 1999; Pandarinath et al, 1999b; Wasson et al, 1983; Juyal et al, 2003). It is, therefore, inferred that groundwater recharged around LGM in the Aravalli foothills and subsequently migrated to its present position within Cambay Basin corresponds to the central (QQ') high fluoride groundwater belt. The groundwater, with relatively low fluoride concentration, on either side of QQ' suggests recharge during relatively less arid climatic regime. The first low fluoride zone between the eastern (RR') and central (QQ') high fluoride belts (^{14}C age 5 – 15 kaBP) is then an indication of groundwater recharged during climatic amelioration (higher precipitation and/or decreased dry deposition and/or reduced evaporation). The next low fluoride groundwater zone in between central (QQ') and western (PP') high fluoride belts is also an indication of groundwater recharged during ameliorated climatic condition prevalent during 25 – >35 kaBP, as indicated by ^{14}C age.

The eastern high fluoride belt (RR') located in the recharge area corresponds to the modern recharge which is an indication that even under the present geo-climatic conditions, groundwater recharged into the regional aquifer system is predisposed to a certain degree of high fluoride content. This is due to combination of (i) leaching; (ii) dry

deposition and evaporation preceding the recharge; and (iii) increased rock-water interaction at higher temperatures during hydrothermal circulation (as evidenced in thermal springs).

The high fluoride-high EC belt (PP') in the western region, indicates the groundwater recharged during previous arid climate phase (^{14}C age >35 kaBP; ^4He age 45-110 kaBP, depending on helium release factor). However, sudden increase in fluoride concentration (from <2 ppm to >6 ppm) and EC (from <2 mS to >8 mS) in the shallow unconfined groundwater around PP' suggests a causal mechanism other than just increased aridity in the past and/ or progressive leaching. The line PP' overlies a low lying tract linking LRK-NS-GC which is a convergence zone for surface and subsurface drainage. The very high level of groundwater fluoride concentration in this belt is possibly due to evaporative enrichment of salts in the stagnant water accumulated in the topographically low lying convergence zone and its infiltration into the shallower aquifers.

The high fluoride and EC in the belt SS' linking the regions of thermal springs (Tuwa and Lasundra) to the low lying area around Nalsarovar can be explained as due to steady venting of hydrothermal fluids (with relatively high concentration of ions including fluoride) into the groundwater in the recharge area around Tuwa and Lasundra and the steady movement of the mixed groundwater in the regional aquifer system throughout the Late Quaternary period. The fluoride contribution by the hydrothermal fluids is so significant and steady that the imprints of arid excursions in climate are not identifiable prominently along SS'. Instead a continuous belt of higher fluoride concentration (>1.5 ppm) and high EC (>2 mS) is seen.

4.2.3 Oxygen and Hydrogen Isotopes in Groundwater and Precipitation

With a view to identify the possible signatures of the past aridity as well as source of thermal spring water, oxygen and hydrogen isotope ratios ($\delta^{18}\text{O}$ and δD) in thermal springs and ground waters of NGC region were measured. Isotopic analyses of modern precipitation were also carried out to provide reference for interpretation of the groundwater isotope data.

The amount weighted average values for the modern rainfall in the NGC region (Figure 4.15a and b; Table 4.5) are: $\delta^{18}\text{O} = -4.3 \pm 2.1\text{‰}$, $\delta\text{D} = -33 \pm 16\text{‰}$ and $d\text{-excess} = 1.2 \pm 4.8\text{‰}$. This $d\text{-excess}$ value as well as the slope (7.6 ± 0.6) and the intercept ($-2.9 \pm 2.2\text{‰}$) of the local meteoric water line (LMWL) are lower than the average values of global meteoric water line (GMWL). As discussed above (see Section 2.4), the evaporation of falling raindrops results in lower values of LMWL slope, its intercept and the $d\text{-excess}$, and higher values of $\delta^{18}\text{O}$ and δD in the residual water. Thus, the lower

values of *d*-excess, the slope, and the intercept of LMWL in the NGC region are isotopic imprints of evaporation from falling raindrops under the present semi-arid climatic regime. Any further evaporation of the rain water, during infiltration and groundwater recharge, will further reduce the values of these isotopic parameters in the groundwater.

The $\delta^{18}\text{O}$ vs. δD plot (Figure 4.15c) of groundwater samples from the NGC region shows a cluster of data points having significantly narrower range of variation, than that for precipitation, with average values of both $\delta^{18}\text{O}$ ($-1.2 \pm 1.3\text{‰}$) and δD ($-22 \pm 5\text{‰}$) being higher than that for precipitation. The average value of *d*-excess of all groundwater samples is $-4.5 \pm 11\text{‰}$, which is lower than that for precipitation samples. The lower value of *d*-excess, narrow range and relatively higher values of $\delta^{18}\text{O}$ and δD in groundwater, compared to that in precipitation, indicate mixing of rain water from different events in the soil zone and additional evaporation during its infiltration. The isotopic characteristics of both modern precipitation and groundwater indicate that the semi-arid NGC region is not only predisposed to significant evaporation during rainfall and recharge but its evidence is preserved in groundwater.

Since the NGC region has experienced more arid excursions in the palaeo-climatic history, as registered in sedimentary records (see Section 1.2.6; and 4.2.2 above), it is expected that the groundwater in this region, which is thousands of years old (see Section 4.1.6), may have recorded and preserved the imprints of past aridity. It is seen from the geographical distribution of $\delta^{18}\text{O}$ and *d*-excess of groundwater from NGC region that (Figure 4.16), groundwater around a linear belt (QQ') is characterized by relatively higher values of $\delta^{18}\text{O}$ and lower values of *d*-excess. In view of the expected isotopic modification of the evaporating water as discussed in section 2.4, the groundwater with relatively lower values of *d*-excess and higher values of $\delta^{18}\text{O}$ around QQ' indicate influence of relatively enhanced evaporation of infiltrating water during its recharge compared to the groundwater outside this belt. The ^{14}C age of the confined groundwater around QQ' within the Cambay Basin, representing the time when it was recharged in the identified recharge area, has been estimated (Section 4.2.2) as 15-25 kaBP. The period around 20 kaBP, corresponding to the Last Glacial Maxima (LGM), has also been identified as a period of enhanced aridity in the NGC region (Prasad and Gupta, 1999; Pandarinath et al, 1999b; Wasson et al, 1983; Juyal et al, 2003). Relatively lower *d*-excess and higher $\delta^{18}\text{O}$ values for groundwater around QQ', therefore, represent the signatures of relatively enhanced evaporation resulting from increased aridity in the region around LGM. Thus, the groundwater isotopic signatures corroborate enhanced aridity in the NGC region around period of LGM, as previously inferred from enhanced fluoride concentration and EC of groundwater around QQ'.

It has been shown that the geothermal waters in the NGC region have high fluoride as well as EC and enhanced concentrations of these geochemical parameters around the line SS' are due to continuous admixture of geothermal waters (around thermal springs of Tuwa and Lasundra) to the recharged groundwater (Section 4.2.2 above). The isotopic analyses of geothermal waters (samples marked TS for thermal springs and TA for thermal artesian wells in Table 4.4) and their comparison with other groundwater and modern precipitation samples offer an opportunity to study the possible interaction between the rock matrix and the infiltrating meteoric water. The $\delta^{18}\text{O}$ value of the crustal rocks range between 5–10 ‰ VSMOW (Figure 9.2 of Clark and Fritz, 1997) whereas most meteoric waters have $\delta^{18}\text{O}$ values <0 ‰. Although hydrogen has a much lower crustal abundance, it is present in several rock forming minerals. Unlike ^{18}O , the greatest enrichment of ^2H is observed in water, while mineral and rocks are preferentially depleted. This contrasting behavior of the two isotopes is important in the isotopic evolution of water in high temperature systems. In the case of the NGC region, the modern precipitation has average $\delta^{18}\text{O} = -4.3 \pm 2.1$ ‰; and the average of all groundwater samples, including geothermal waters, is $\delta^{18}\text{O} = -1.2 \pm 1.3$ ‰.

The thermal springs at Lasundra and Tuwa are seen to be slightly enriched (average $\delta^{18}\text{O} = -1.4 \pm 0.4$ ‰, for 6 samples) compared to ground waters in the surrounding region. On the other hand, $\delta^{18}\text{O}$ values of thermal artesian wells on the western flank do not show much difference (average $\delta^{18}\text{O} = -2.4 \pm 1.0$ ‰ for 8 samples) compared to the other groundwater samples in NGC region. With exchange induced enhancement of $\delta^{18}\text{O}$ and decrease of δD , one can expect a reduction in the *d*-excess values of thermal waters. The thermal springs from the eastern flank have *d*-excess = -4.1 ± 3.2 ‰ and thermal artesian wells on the western flank have *d*-excess = -6.5 ± 7.3 ‰. Statistically these averages are not distinguishable from the average groundwater values for the entire NGC region, but local enrichment of ^{18}O and lowering of *d*-excess in the areas with thermal waters is seen in Figure 4.16. Thus isotopic evidence of water-rock interaction in geothermal waters of the NGC region is indicated, but is not so unambiguous. The evidence is, however, clearer in case of thermal springs of Tuwa and Lasundra.

It may be noted that the $\delta^{18}\text{O}$ enrichment in groundwater around QQ', discussed earlier, is not related to any geothermal activity and also did not show any enhanced helium concentration. Whereas, the geothermal waters on both flanks have higher helium concentration (Section 4.1.1).

It is, therefore, inferred that the $\delta^{18}\text{O}$ in thermal springs at Tuwa and Lasundra show a trend towards isotopic equilibrium between ^{18}O depleted meteoric water and ^{18}O enriched rocks at higher temperatures. This also fits in with the conceptual tectono-hydrothermal model as described in Section 4.2.1.

4.2.4 Groundwater Ages

4.2.4.1 ^{14}C Ages

The estimated groundwater ^{14}C ages are seen (Figure 4.17) to increase progressively from <2 kaBP (along Aravalli foothills) to >35 kaBP in the low-lying tract linking LRK-NS-GC. Farther west, lower ^{14}C ages are found, but only in two groundwater samples (CBGW-344, -351; Table 4.6). The low lying LRK-NS-GC tract is the zone of convergence for the surface drainage (see Section 1.2.5; Figure 1.5). Presence of several free flowing artesian wells found in the LRK-NS-GC tract and continuity of the aquifers with those from the Cambay Basin confirm that their recharge area is in the foothills of Aravalli Mountains. It is seen (Figure 1.6) that succession of sand/ silty-clay layers is roughly inclined parallel to the ground surface and the sampled tube wells tap nearly the same water bearing formations across the NGC region. Since the tubewells tap all the water bearing horizons intercepted within their maximum depth, these are treated as pumping a single aquifer system for which the ^{14}C ages increase progressively in the flow direction. The above geo-hydrological model appears reasonable because, the unconfined aquifers in the region have almost completely dried up (as evident from several dried up and abandoned dug wells). Therefore, the groundwater in all the parallel layers of confined aquifers is recharged largely from the sediment-rock contact zone in the foot hills of Aravalli Mountains, and after the confinement becomes effective, moves with nearly the same velocity. The narrow range of $\delta^{13}\text{C}$ values of TDIC of groundwater (Table 4.6) indicates that the dead carbon dilution factor for the various samples is not significantly different from each other. As a result, the relative age difference between the samples can be relied upon. The only sample, with much lower $\delta^{13}\text{C}$ value (-21.4‰) is derived from a very deep aquifer from the Gundi village (CBGW-358; Table 4.6) and showed age beyond ^{14}C dating limit. The low redox potential (10 mV) of this sample suggested possible CO_2 contribution from its anaerobic oxidation.

From hydro-geological considerations (see Section 1.2; Figure 1.6), it seems that confinement of the regional aquifer in the NGC region becomes effective near the ECBBF around the ^{14}C age contour of ~2 kaBP. Within the Cambay Basin, the age isolines are nearly parallel to each other and the horizontal distance between the successive 5 kaBP isolines is nearly constant giving a regional flow velocity in the range

2.5 – 3.5 m a⁻¹ for the prevailing hydrostatic gradient of 1 in 2000 (GWRDC, unpublished data), which is comparable to an earlier estimate of ~ 6 m a⁻¹ (Borole et al, 1979) for a small part of the Vatrak-Shedhi sub-basin (marked by an ellipse in Figure 4.17). The Vatrak-Shedhi sub-basin is closer to the recharge area, therefore, both the permeability and the hydraulic gradient are expected to be relatively higher than that for the regional estimates of flow velocity (2.5 – 3.5 m a⁻¹) from this study.

4.2.4.2 ⁴He Ages

As seen from Figure 4.1 and Figure 4.18, the 5 ppmAEU He_{ex} isoline runs along the WCBBF and corresponds to ⁴He age of ~ 15 kaBP (for helium release factor; $\Lambda_{\text{He}} = 1$), and ~ 37 kaBP for $\Lambda_{\text{He}} = 0.4$. The ⁴He ages (Figure 4.18) for $\Lambda_{\text{He}} = 0.4$ are in close agreement with the ¹⁴C ages (Figure 4.17) when no crustal flux is considered, except for pockets of anomalous groundwater helium concentrations. This is supported by other studies, which indicate that relatively young ground waters are dominated by the *in-situ* production of ⁴He. Torgersen and Clark (1985) found good concordance between ¹⁴C and ⁴He ages of groundwater in the Great Artesian Basin, Australia, up to ~ 50 kaBP. Kulongoski et al (2003) found a good correlation between ¹⁴C and ⁴He ages of groundwater up to ~25 kaBP in the Mojave River Basin, California. They explained the result by existence of wells in the basin at shallow depth and hence, above the influence of crustal ⁴He flux. A similar situation also prevails in the NGC region up to the WCBBF. In the NGC region, the fluvial deposits grade from coarse grain sizes near the Aravalli foothills (recharge area) to fine grain sizes near the LRK-NS-GC region. This is also indicated by a rapid decrease in aquifer transmissivity from ~ 1000 m²d⁻¹ east of the ECBBF to < 200 m²d⁻¹ west of the WCBBF (GWRDC, unpublished data). Thus, greater transmissivity of the aquifers up to WCBBF of the NGC region may result in groundwater flow that entrains negligibly small basal crustal flux, thereby leaving groundwater ⁴He ages virtually unaffected by the deep crustal ⁴He flux.

As mentioned above (see Section 2.6.2), there is some uncertainty on the calculated He_{ex} that is dependent upon estimation of (i) excess air; and (ii) dissolved helium in solubility equilibrium with the atmosphere. Depending on the physical nature of capillary fringe zone just above the saturated zone, air bubbles can be entrapped and transported into the saturated zone by infiltrating water. The air bubbles can also be entrapped by rapid rise in the water table due to occasional heavy rainfall in semi arid regions. Dissolution of such air bubbles into the groundwater introduces excess-air and consequently all its components including helium (⁴He_{ea}). The presence of 'excess air' in groundwater results in observed ⁴He concentrations (⁴He_s) to be higher than those

expected from solubility equilibrium (${}^4\text{He}_{\text{eq}}$) (Heaton and Vogel, 1981; Stute and Schlosser, 1993; Aeschbach-Hertig et al, 2000). In the present study it was not possible to correct for the 'excess air' since neon concentrations were not measured. According to laboratory column experiments on the formation of 'excess air' in quasi saturated porous media (Holocher et al, 2002), the amount of 'excess air' can range from 1% to 16% of the equilibrium solubility concentration. However, in field studies higher Neon excesses have also been found (Heaton and Vogel, 1981; Aeschbach-Hertig et al, 2002).

Since the solubility of helium is relatively insensitive to temperature (Ozima and Podosek, 1983), variation in the temperature of recharge water has a small effect on ${}^4\text{He}$ dissolved in solubility equilibrium with atmosphere (${}^4\text{He}_{\text{eq}}$), which can be estimated from the regional climate and groundwater temperature. The mean annual temperature of recently recharged groundwater in the Aravalli foothills is 30 ± 5 °C, as a result ${}^4\text{He}_{\text{eq}}$ can decrease by ~10% relative to the groundwater recharged in relatively colder climate.

Thus, both ${}^4\text{He}_{\text{eq}}$ and ${}^4\text{He}_{\text{ea}}$ would lead a systematic error of ~+10% and ~-20%, respectively on the atmospheric air equilibration value of 5.3 ppmAEU which is subtracted from the measured ${}^4\text{He}$ in groundwater samples to calculate ${}^4\text{He}_{\text{ex}}$ (see Section 2.6.2). While corrections due to recharge temperature and 'excess air' are important for precise groundwater age estimation, particularly in case of low ${}^4\text{He}$ concentration samples, the conclusion for high ${}^4\text{He}$ concentrations are not significantly affected by such corrections. Considering this, and the fact that accuracy of measurement for low helium concentrations is ~20%, the error on ${}^4\text{He}$ ages can be as high as 50% for groundwater samples which have <5 ppmAEU ${}^4\text{He}_{\text{ex}}$. Therefore, the isolines for ${}^4\text{He}_{\text{ex}}$ values <5 ppmAEU are not shown in Figure 4.1 and the conclusions are based only on samples with ${}^4\text{He}_{\text{ex}} \geq 5$ ppmAEU.

It is seen from Figure 4.1 that ${}^4\text{He}$ concentrations rapidly increase west of the 5 ppmAEU ${}^4\text{He}_{\text{ex}}$ isoline that almost coincides with WCBBF. This could be due to (i) rapidly increasing residence time of groundwater resulting from decrease in the transmissivity as a result of a general decrease in grain size away from the sediment source; and/or (ii) increase in the influence of deep crustal flux of helium in the aquifer. The latter possibility is supported by very high (>50 ppmAEU) ${}^4\text{He}_{\text{ex}}$ pockets on both eastern and west flanks of the Cambay Basin. The east flank is the major recharge area of aquifers in the Cambay Basin where groundwater pockets of very high helium are associated with the thermal springs of Tuwa and Lasundra. Considering the observed ${}^4\text{He}_{\text{ex}}$ as *in-situ* produced will result in groundwater age >100 kaBP, which is not tenable hydro-geologically. The presence of extraneous ${}^4\text{He}$ in these pockets is also indicated by the overlapping of high groundwater temperature (>35°C) pockets suggesting hydrothermal

venting of deep crustal fluids in such pockets. The ^4He method of dating is not applicable for groundwater in such pockets.

The deep crustal He flux may also affect the aquifer by diffusion from the underlying basement followed by entrainment and upward migration, particularly towards the discharge region of the aquifer (Bethke et al, 2000). Thus, higher amount of the crustal flux may be entrained with increasing distance along flow paths, resulting in a rapid increase in the helium concentration towards the discharge region. For the five samples west of the WCBBF for which ^{14}C groundwater ages (Figure 4.17) are also measured, a ^4He crustal flux of $\sim 1.5 \times 10^{-8} \text{ cm}^3 \text{ STP He cm}^{-2} \text{ y}^{-1}$ produces an agreement between the two dating methods. This, however, ignores *in-situ* production. Considering finite *in-situ* production due to U and Th in the aquifer matrix, the ^4He crustal flux must $\ll 1.5 \times 10^{-8} \text{ cm}^3 \text{ STP He cm}^{-2} \text{ y}^{-1}$. However, for the Lasundra and Tuwa thermal springs in the East Flank and pockets of very high helium on the West flank of Cambay Basin a crustal flux $> 10^{-6} \text{ cm}^3 \text{ STP He cm}^{-2} \text{ y}^{-1}$ is necessary for agreement between ^4He and ^{14}C ages. Takahata and Sano (2000) reported ^4He crustal flux of $3.0 \times 10^{-8} \text{ cm}^3 \text{ STP He cm}^{-2} \text{ y}^{-1}$ from a sedimentary basin in Japan. The typical continental ^4He flux is $3 \times 10^{-6} \text{ cm}^3 \text{ STP He cm}^{-2} \text{ y}^{-1}$ (O'Nions and Oxburgh, 1983). It is thus seen that the observed pattern of high helium concentrations in localized pockets can only be explained by invoking 2-3 orders of magnitude variation in crustal diffusion flux which is another way of saying that crustal diffusion occurs along preferred pathways formed by deep seated basement faults. The rising arm of the convective hydrothermal circulation, also formed along these faults, introduces this non *in-situ* component of ^4He in the form of a plume into groundwater where pockets of He_{ex} are observed. Thus, the possible role of the crustal flux also fits into the tectono-hydrothermal model described above (Section 4.2.1).

In case of groundwater outside the pockets of very high He_{ex} , the *in-situ* ^4He accumulation, even without crustal flux correction, produces a reasonable correspondence between ^{14}C and ^4He ages within the 50% uncertainty range. For samples from the west of the WCBBF, a low crustal flux value of $< 1.5 \times 10^{-8} \text{ cm}^3 \text{ STP He cm}^{-2} \text{ y}^{-1}$ can not be ruled out as invoking it produces a better agreement with the few definite ^{14}C groundwater ages. Farther west, ages must be $> 45 \text{ kaBP}$, possibly as old as 100 kaBP .

4.2.4.3 $^4\text{He}/^{222}\text{Rn}$ Ages

The measured ^{222}Rn activity in the NGC region (Table 4.7) showed a variation of $\pm 50\%$ around an average value of $\sim 800 \text{ dpm/l}$ (except the thermal spring water at Tuwa) suggesting a similar range of variation in the U concentration of the aquifer material. This

range of U variation was also seen in the analyzed drill cutting samples and on shallow depth sediments from the NGC region (Srivastava et al, 2001; Agarwal et al, 2006).

As explained earlier (see Section 2.6.3), the $^4\text{He}/^{222}\text{Rn}$ ages (Table 4.7; Figure 4.19) are independent of porosity, density and U concentration but depend on Th/U of the aquifer material. Additionally, the $^4\text{He}/^{222}\text{Rn}$ ages also depend on the release factor ratio ($\Lambda_{\text{Rn}}/\Lambda_{\text{He}}$). As in the case of ^{14}C ages (Figure 4.17), a gradual $^4\text{He}/^{222}\text{Rn}$ age progression from the recharge area towards the WCBBF is observed in major part of the study area (Figure 4.19). These $^4\text{He}/^{222}\text{Rn}$ ages were obtained using $\Lambda_{\text{Rn}}/\Lambda_{\text{He}} = 0.4$ to give the best match with the ^{14}C age gradient across the Cambay basin. This gradient matching approach was chosen because the inferred groundwater flow velocities in the confined aquifer by the two methods match only when age gradients match. This also ensures that various uncertainties in the age estimation related to (i) the initial activity of ^{14}C (A_0) in the recharge area; (ii) ^4He dissolved in solubility equilibrium at recharge temperature ($^4\text{He}_{\text{eq}}$); and (iii) dissolved ^4He due to 'excess air' have as little influence on matching as possible. A radon release factor (Λ_{Rn}) ranging from 0.01-0.2 has been indicated from laboratory experiments for granites and common rock forming minerals (Krishnaswami and Seidemann, 1988; Rama and Moore, 1984). Based on measured values of uranium concentration and ^{222}Rn activity, the value of Λ_{Rn} is estimated to be 0.15 ± 0.07 (using Eq. 2.31 and 2.32), which is consistent with the literature. On the other hand for ^4He , Torgersen and Clarke (1985), in agreement with numerous other authors have suggested $\Lambda_{\text{He}} \approx 1$. For $\Lambda_{\text{Rn}} = 0.15 \pm 0.07$ and $\Lambda_{\text{Rn}}/\Lambda_{\text{He}} = 0.4$, $\Lambda_{\text{He}} = 0.4 \pm 0.3$ is obtained for best regional matching between $^4\text{He}/^{222}\text{Rn}$ (Figure 4.19) and ^{14}C ages (Figure 4.17). This is shown in Figure 4.21 where age progression along the line BB' (drawn in Figure 4.17, Figure 4.18 and Figure 4.19) is plotted. The arrow in the middle of each trapezoid shows the median value of the model age by the respective method. The progressively increasing width of the trapezoid depicts the estimated error at any given median age. The slopes of the respective median lines give the age gradients. It is seen that for $\Lambda_{\text{He}} = 0.4$, both ^4He and $^4\text{He}/^{222}\text{Rn}$ age gradients matches the ^{14}C age gradient. In view of the various uncertainties that affect the three methods, the ^{14}C method appears to be the most reliable one in the present case. Firstly, because the $\delta^{13}\text{C}$ values of TDIC show a very narrow range ($-9.6 \pm 1.2 \text{‰}$) and secondly, the ^{14}C age iso-lines show a nearly parallel distribution, approximately in agreement with the distribution of transmissivity of the aquifers obtained from the pumping test data, progressively decreasing from $\sim 1000 \text{ m}^2 \text{ d}^{-1}$ east of the ECBBF to $< 200 \text{ m}^2 \text{ d}^{-1}$ west of the WCBBF (GWRDC, unpublished data). Therefore, considering ^{14}C age data as reference, the best match for both $^4\text{He}/^{222}\text{Rn}$ and ^4He ages is obtained for $\Lambda_{\text{He}} = 0.4$, so that the 5 ppmAEU

He_{ex} iso-line (Figure 4.18) corresponds to 4He groundwater age of ~37 kaBP (instead of ~15 kaBP).

A value of $\Lambda_{He} < 1$ in NGC region would appear contrary to the apparent $\Lambda_{He} > 1$ due to release of geologically stored helium in young sediments derived from old protoliths (Solomon et al, 1996).

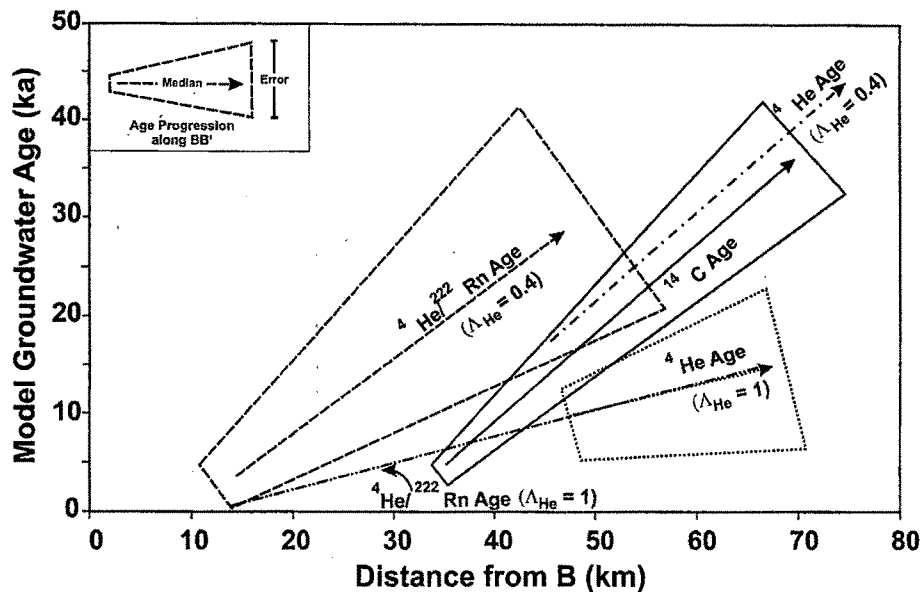


Figure 4.21 Plot of groundwater age progression along line BB' (shown in Figure 4.17, Figure 4.18 and Figure 4.19) for comparing the age gradients for model ^{14}C ages, 4He ages for $\Lambda_{He} = 1$ and $^4He/^{222}Rn$ ages both for $\Lambda_{He} = 1$ and $\Lambda_{He} = 0.4$.

The comparatively low estimate of Λ_{He} can either be due to (i) loss of 4He from the aquifer system, or (ii) incomplete release of radiogenic 4He from the grains over time scales of ~100 kaBP. The former possibility is contrary to the basic assumptions of both 4He and $^4He/^{222}Rn$ dating methods. The latter possibility may not be ruled out because the depositional age of aquifer material in the Cambay Basin is Late Quaternary (Pandarinath et al, 1999; Prasad and Gupta, 1999) and it is possible that all the helium produced in the aquifer material, since deposition, is only partially released to the interstitial water. Contrary to Solomon et al. (1996), this would require a mechanism that nearly releases all of the geologically stored helium in the grains due to mechanical/ thermal/ chemical stress during the process of weathering & transportation and subsequent build up within the grains with a partial release to interstitial water during the quiet post depositional period until a steady-state (for helium loss) is achieved within individual grains. The possibility of partial release of helium is justified since the grain size (> 0.5 mm) of aquifers forming horizons is considerably larger compared to the

recoil path length (30–100 μm) for ^4He . Recoil of the decaying atom from the outer surface of the grain is one of the mechanism by which radioactive products in solids enter the pore fluid. (Torgersen, 1980; Gupta et al, 2002). Thus, the possibility of partial release of helium is justified; however, more definitive arguments concerning the involved mechanisms is not possible based on the present data. In fact, the use of groundwater helium for earthquake prediction (Sano et al, 1998) is based on the premise that in the normal course Λ_{He} may be <1 .

In this Chapter results from various isotopic and geochemical investigations, and the discussion leading to specific conclusions were presented. In the Chapter 5 next, the summary and conclusions of this study are presented and the important contributions and advancements in the understanding of geohydrological processes operating in the NGC region are highlighted.